TADPOLE-IMPROVED SU(2) LATTICE GAUGE THEORY

by

Norman Harold Shakespeare

B.Sc., University of Winnipeg, 1994

THESIS SUBMITTED IN PARTIAL FULFILMENT OF

THE REQUIREMENTS FOR THE DEGREE OF

MASTER OF SCIENCE

in the Department of Physics

SIMON FRASER UNIVERSITY

December 1996

ISBN 0-612-17102-7

PARTIAL COPYRIGHT LICENSE

I hereby grant to Simon Fraser University the right to lend my thesis, project or extended essay (the title of which is shown below) to users of the Simon Fraser University Library, and to make partial or single copies only for such users or in response to a request from the library of any other university, or other educational institution, on its own behalf or for one of its users. I further agree that permission for multiple copying of this work for scholarly purposes may be granted by me or the Dean of Graduate Studies. It is understood that copying or publication of this work for financial gain shall not be allowed without my written permission.

Title of Thesis/Project/Extended Essay

Tadpole-Improved SU(2) Lattice Gauge Theory

Author: _____
(signature)

Norman H Shakespeare
(name)

9 December 1996
(date)

Approval

Name:	Norman Harold Shakespeare
Degree:	Master of Science
Title of Thesis:	Tadpole-Improved SU(2) Lattice Gauge Theory
Examining Committee:	Dr. L. E. Ballentine (Chairperson)

Dr. H. D. Trottier
Senior Supervisor
Assistant Professor, Department of Physics

Dr. D. H. Boal
Professor, Department of Physics

Dr. K. S. Viswanathan
Professor, Department of Physics

Dr. R. M. Woloshyn
Research Scientist
TRIUMF, UBC, Vancouver, B. C.

Dr. B. K. Jennings
Internal Examiner
Research Scientist
TRIUMF, UBC, Vancouver, B. C.

Date Approved: 3 December 1996

Abstract

Lattice Quantum Chromodynamics is a cornerstone of phenomenology for low-energy strong interactions. This thesis deals with new algorithms which may allow the use of larger lattice spacing in numerical simulations of QCD.

Traditionally lattice calculations have been done using a Wilson action where the lattice spacing has been kept in the 0.10 fm range to achieve good accuracy. In this research calculations are performed using an action where leading discretization errors in the Wilson action are removed. This so-called tadpole-improved action is used on coarse lattices to make new calculations in SU(2) colour. The efficiency of these calculations is increased by using anisotropic lattices whereby the temporal spacing is smaller than the spatial. A "fuzzing" technique is used to enhance the signal by smearing the straight line lattice link with other nearby paths.

The specific calculations are for the lattice anisotropy, the static quark potential, the scalar glueball mass and the tensor glueball mass. Both Wilson and tadpole-improved actions are used on coarse lattices with spacings in the range of about 0.2 fm to 0.4 fm.

The lattice anisotropy shows much less renormalization for the tadpole-improved action than for the Wilson action. As well, breaking of rotational invariance is much smaller for the tadpole-improved action. The scalar glueball mass is substantially closer to the continuum value for the tadpole-improved action than the Wilson action. Preliminary results for the tensor glueball mass are obtained, but no statistically significant difference is observed between the two actions.

Dedication

To Karen

Acknowledgments

I would like to thank Dr. Trottier for accepting me as one of his graduate students and for all of his support during this project.

Thanks also to the staff and faculty of the Physics Department for all the help and encouragement.

Contents

List of Tables

List of Figures

Chapter 1

Introduction

Lattice Quantum Chromodynamics (QCD) has become a cornerstone of phenomenology for low-energy strong interactions. Perturbative methods for solving a quantum field theory like Quantum Electrodynamics (QED) fail for treating QCD at low energies or large distances, where the running coupling constant $\alpha_s(r)$ becomes large. Lattice QCD offers a truly non-perturbative technique for studying low energy phenomenology. The techniques of lattice QCD readily lend themselves to computer simulation. Since the mid-1970's when the gauge invariant lattice action was introduced by Wilson [1], the main concern of theorists has been getting fast enough computers to obtain numerical solutions of full QCD. This thesis deals with newly developed methods to reduce the amount of computer time needed to solve QCD problems.

The main ingredient of the cost of doing a lattice simulation on the computer is the lattice spacing (usually denoted by a). The length (L) of a side of the lattice is L=na where n is the number of lattice points on a side. The physical volume of the four-dimensional lattice is L^4 and, in order to keep the physical volume fixed, the length L must be fixed as $a \to 0$. Therefore the total number of points in the lattice is proportional to $1/a^4$. Furthermore the lattice spacing (a) does not appear explicitly either in the action or in the observables computed from the simulation. Therefore, the length of an observable in lattice units, $\zeta = l/a$,

diverges as $a \to 0$, where l is the physical length. Diverging correlation lengths are a hallmark of second order phase transitions and thus it is expected that auto-correlation functions will exhibit critical slowing down. The number of updates required to generate an uncorrelated member of the ensemble of quantum states, near a critical point, typically diverges as $1/a^2$. (See for example reference [2]). Hence the total cost of doing a computer simulation will scale as $1/a^6$.

In order to keep the cost down it is therefore desirable to use as large a lattice spacing as possible. However, errors are introduced in moving from the continuum to the discrete lattice and, the larger the lattice spacing, the larger are these errors. Over time, a consensus has emerged that lattice spacings should be kept in the 0.05 fm to 0.10 fm range to minimize these errors and have reliable results. (For a pedagogical review see, for example, reference [3].) Unfortunately, this requires enormous lattices to achieve adequate physical volume. For example a 32^4 lattice at 0.05 fm spacing has a modest volume of $(1.6 \text{ fm})^4$ bearing in mind that a typical length scale for confinement is about 1 fm, the "radius" of a proton. This then equates to supercomputing.

1.1 Tadpole Improvement

Consider solving a classical field theory on a lattice, for example Coulomb's law, $-\nabla^2 A_0 = \rho$. At leading order in a, the derivatives are defined by finite differences. In the example $\partial_i A^0(x) = (A^0(x+\hat{i}a) - A^0(x-\hat{i}a))/2a + O(a^2)$. A better approximation, eliminating the $O(a^2)$ errors, can be obtained using next-to-nearest neighbour couplings. A similar approach can be tried for a discrete version of a quantum field theory. However, in a quantum field theory there are large ultraviolet fluctuations ($A_\mu \sim 1/a$) which can spoil such power counting in a. In order to remove these effects which actually generate the leading

order discretization errors in the conventional lattice actions (usually referred to as Wilson actions), a technique called tadpole improvement was originally suggested by Lepage and Mackenzie in 1993.[4] The ultraviolet fluctuations come from so-called tadpole diagrams that are induced by a non-linear connection between the lattice quantum fields and the standard continuum gauge fields. Tadpole improvement largely removes these ultraviolet fluctuations by doing a mean field renormalization of the lattice quantum fields.

One of the first and most thorough applications of this technique has been the calculations of the upsilon [5] and charmonium [6] spectra by Davies and collaborators in 1994 and 1995, where leading discretization errors in a heavy quark action were removed. However, the gluonic action was not improved in these calculations and so the lattice spacing was kept relatively small.

It was more recently demonstrated that tadpole improvement could be used to remove discretization errors in both the gluonic and quark actions in order to work on very coarse lattices. In 1995, Alford and collaborators computed the SU(3) static quark potential on a coarse lattice with spacing of 0.4 fm and found that rotational invariance was broken by 40% in the Wilson theory but only 2-4% in the improved theory.[7] In the same research paper they also looked at the spin-averaged charmonium spectrum. Using an improved action for the lattices with spacings of 0.40 fm, 0.33 fm and 0.24 fm, they found that the spectrum agreed within errors to a Wilson action calculation on a lattice with spacing of 0.17 fm.

In 1996, Fiebig and Woloshyn analyzed light hadron masses using a tadpole-improved action. For the ratio of nucleon to ρ-meson mass, the improved action values at 0.3 fm and 0.4 fm agree with the Wilson action at smaller lattice spacing ($\lesssim$ 0.1 fm).[8] Light hadron spectroscopy has also been done by Alford *et al* [9] and by Collins *et al* [10].

Hadrons are made up of more elementary particles called quarks. The gauge particles that provide the strong binding force between the quarks are called gluons. The gluons carry a colour "charge" and can interact directly with each other. Due to confinement, a state with

net colour can never be seen; however, colour-singlet combinations of gluons ought to have finite energy. These bound states of gluons are referred to as gluonium or more commonly as glueballs. By studying the pure gauge sector and ignoring the effects arising from virtual quarks an approximation of the glueball mass can be achieved.[11]

In 1995 Morningstar and Peardon used a tadpole-improved action to examine the SU(3) scalar glueball spectrum.[12] They found a significant reduction in the finite lattice spacing errors in the glueball mass. However the large lattice spacing in the "temporal" direction limited the number of statistically useful mass measurements. More recently they repeated SU(3) glueballs on an anisotropic lattice.

1.2 Anisotropic Lattice

The efficiency of certain lattice calculations can be enhanced by using a smaller lattice spacing for the "temporal" direction a_t than for the "spatial" directions a_s. For an example, the scalar glueball correlation function falls off exponentially with Euclidean time as $e^{-M_g T}$ while the statistical noise is fairly constant. The idea is to get more measurements at smaller physical T before the signal disappears into the noise. Therefore it is more efficient here to use a smaller "temporal" lattice spacing than to do additional Monte Carlo measurements on an isotropic lattice.

For an anisotropic lattice the bare input value of anisotropy, a_t/a_s, is never equal to the measured value of anisotropy. The reason is that the bare input value is renormalized by quantum effects. In an anisotropic lattice action there are two different couplings. One coupling multiplies terms sensitive only to the "spatial" length scale a_s. The other coupling multiplies terms sensitive to both a_s and a_t. These two couplings can (and do) behave differently as these lattice spacings are sent to zero, and this shows up as a "renormalization" of the input anisotropy. Pioneering theoretical work was done by A. Hasenfratz and P.

Hasenfratz [13] in 1981, and by F. Karsch [14] in 1982. In 1988 Burgers et al. showed numerically that these renormalizations can have large effects on the anisotropy.[15] Alford et al. showed in 1996 that tadpole-improvement removed most of these renormalizations.[16] Some preliminary results obtained in this thesis have been reported in that work.

Following this work, in 1996 Morningstar and Peardon used coarse anisotropic lattices with tadpole-improved actions to examine SU(3) glueball masses.[17] In this research, they required much smaller statistical samplings to resolve the glueball correlators than in their previous isotropic work.[12] Using an anisotropy of 1/3 with tadpole-improvement they found that to get similar accuracy they required two to three orders of magnitude fewer calculations than were needed on Wilson actions which used much smaller lattice spacings.

1.3 Fuzzing

Fuzzing is a technique that has been successfully used to reduce the noise and enhance the signal in lattice simulations. In a lattice formulation of QCD the gauge fields are replaced by "links" which "transport" the phase of a quark (or gauge) field from one site to another. In fuzzing the straight line lattice link is smeared with other nearby paths. In some calculations, for example the mass of the glueball, the simplest operators are constructed from small loops which are generally the size of the smallest cell on the lattice while the objects being measured tend to be several lattice spacings in size. The idea is to make operators that are closer to the size of the physical object being measured and thus to increase the overlap with the ground state. The Teper fuzzing method is described in reference [18]. In this research I use the APE collaboration iterative method to get these smeared or fuzzy operators.[19]

1.4 Research Calculations

The work done for this thesis has been lattice gauge theory simulations under SU(2) colour. SU(2) shares many features with SU(3), like confinement and glueball states. Therefore SU(2) provides a cheaper laboratory for studying this physics. There is a long history of such calculations. For example in 1992 the UKQCD collaboration undertook a large scale study of potentials to help understand the limit of lattice QCD as the spacing goes to zero. [20] They used a 48^3 x 56 SU(2) lattice with a spacing of 0.028 fm.

The specific calculations in this thesis are the lattice anisotropy, the static quark potential, the mass of the scalar glueball and the mass of the tensor glueball. This thesis contains the first calculations of these quantities using the SU(2) tadpole-improved action.

Computations have been done to determine these quantities, for both standard Wilson actions and tadpole-improved actions, and then to compare the results over a range of lattice spacings. The calculations were done on lattice spacings ranging from 0.1 fm to 0.4 fm. The glueball masses were compared with the published results of research using lattices with small lattice spacing. The strategy was to quantify the gains in reliability of results from the tadpole-improved actions compared to the standard Wilson action at large lattice spacing.

The material in this thesis has been organized as follows. In the following chapter I establish the basic theoretical framework for lattice gauge theory, leading from the Feynman path integral to the Wilson loops. In this same chapter the methodology for obtaining the static quark potential is detailed. The potential is used to resolve the lattice spacing. At the end of the chapter I describe the mechanics of the numerical simulations which are used to calculate the observables. In chapter 3 the methods to eliminate leading discretization errors are

developed. This includes the removal of leading discretization errors both at the classical field theory level (classical improvement) and at the quantum level (tadpole improvement). In chapter 4 I develop the physics of the anisotropic lattice including a procedure to ascertain the measured anisotropy. Theoretical background and the methodology for obtaining the glueball mass is introduced in chapter 5. The technique of fuzzing is illustrated in chapter 6 along with results from fuzzing trials. Chapter 7 contains the detailed results from the simulations. This includes the first calculations using the SU(2) tadpole-improved action for lattice anisotropy, static quark potential, scalar glueball mass and tensor glueball mass. Wilson action values, from both the literature and my own simulations, are presented and compared with the tadpole-improved values. The last chapter gives the final conclusions.

Chapter 2

Wilson Lattice Action

In lattice QCD, continuous space and time are replaced by a discrete 4-dimensional rectangular grid with side length L and lattice spacing a. The lattice sites are designated by their position $x = (x^1, x^2, x^3, x^4)$. Typically the lattice directions are denoted by μ, ν which are also used as the corresponding unit vectors. The quark fields 'live' on the lattice sites while the gluon fields 'live' on the so-called "links" which join adjacent lattice sites. The quantized theory is defined through a Feynman path integral using a gauge invariant action based on the lattice gauge fields. For computation it is most convenient to use the Euclidean path integral as shown in the next section. The gauge fields on the lattice are the link variables which are elements of the gauge group and are related to the continuum gauge potential as developed in the link variables section. The static interquark potential can be computed by calculating the expectation value of a gauge invariant quantity, called a Wilson loop, built only from the gauge fields. This is investigated in the subsequent section along with the breaking of rotational invariance. To make the problems tractable, statistical methods are employed (specifically the Monte Carlo simulation) as described in the final section of the chapter.

2.1 Feynman Path Integrals

The Feynman path integral is equivalent to solving the Schrödinger equation. In one-dimensional quantum mechanics the amplitude to go from an initial space-time point (x_i,t_i) to a final space-time point (x_f,t_f) can be given in terms of the Feynman path integral

$$K(x_f t_f ; x_i t_i) = \int_{(x_i,t_i)}^{(x_f,t_f)} D[x(t)]\ e^{\frac{i}{\hbar}S(x(t))}$$

where $\int D[x(t)]$ means the sum over all paths from (x_i,t_i) to (x_f,t_f).

2.1.1 Euclidean Time

One drawback to using the Feynman path integral in numeric computation is that in Minkowski space-time the factor e^{iS} causes high frequency oscillations. The action is

$$iS = i\int_{t_i}^{t_f} L(x(t),\dot{x}(t))\ dt$$

and changing to Euclidean space-time and letting $t \rightarrow -i\tau$ this action becomes

$$iS = -\int_{\tau_i}^{\tau_f} L_E(x(\tau),\dot{x}(\tau))\ d\tau$$

where $L_E = \frac{1}{2}m\left(\frac{dx}{d\tau}\right)^2 + V(x)$. Then the propagator becomes:

$$K(x_f\tau_f; x_i\tau_i) = \int_{(x_i,\tau_i)}^{(x_f,\tau_f)} D[x(\tau)]\ e^{-S(x(\tau))}$$

which has exponential damping. This is easier to deal with than the high frequency oscillations in the action of Minkowski space-time. Therefore changing to Euclidean time where $x^0 \rightarrow -ix^4$ is desirable.

2.2 Link Variables

Let the continuum gauge potential be denoted by $A_\mu(x) = A_\mu^{\ b}(x)\ \frac{\sigma_b}{2}$ where σ_b are the Pauli matrices. The definition of the lattice link variable $U_\mu(x)$, which "joins" site x to an adjacent site $x + \mu$, is given by:

$$U_\mu(x) = \underline{P}\ e^{\,i \int_x^{x+a\hat{\mu}} g A_\mu(x')\, dx'}$$

where $\underline{P}$ is a path ordered product.

This link variable $U_\mu(x)$ is a directed line from lattice site x to lattice site $x + \mu$. The conjugate link variable $U_\mu^{\dagger}(x)$ represents the directed line in the other direction, namely from $x + \mu$ to x. These are illustrated in figure 2.1.

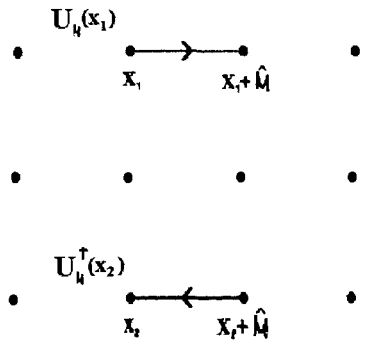

Figure 2.1 Lattice link variables

Whatever the meaning of the path ordered product, in the end $U_\mu(x)$ is a product of SU(2) group elements $e^{i\theta_1 \hat{n}_1\cdot\vec{\sigma}/2}\, e^{i\theta_2 \hat{n}_2\cdot\vec{\sigma}/2} \cdots$ and so can be expressed as some element of the group

$$U_\mu(x) = \underline{P}\, e^{i\int_x^{x+a\hat{\mu}} g A_\mu(x')\, dx'} = e^{i\theta\, \hat{n}\cdot\vec{\sigma}/2}$$

Thus the link variable can also be presented as

$$U_\mu = \cos\left(\frac{\theta}{2}\right)\mathbb{I} + i\sin\left(\frac{\theta}{2}\right)\vec{\sigma}\cdot\hat{n}$$

$$= U(4,\mu,x)\,\mathbb{I} + i\sum_{i=1}^{3} U(i,\mu,x)\,\sigma_i$$

which gives us the constraint $U^2(4) + \sum_i U^2(i) = 1 \quad \forall\ x,\mu$.

2.2.1 Boundary Conditions

The length, L, of a side of the lattice is usually given in terms of the number of lattice spacings n. Therefore L = n a where n is the number of links in the side. The size of the

lattice is then normally given as n^4 or $n^3 \times n_t$ for a lattice where the "temporal" dimension n_t is different from the "spatial" dimension n.

Periodic boundary conditions are used. The boundaries on the lattice are set such that for a dimension of length n, the n + 1 position is identified with position 1. Also the "0" position before position 1 is identified with position n. In other words the lattice wraps around on itself like a 4-dimensional torus, for example:

$$U_\mu(x=n_x+1,y,z,t) = U_\mu(x=1,y,z,t)$$

$$U_\mu(x=0,y,z,t) = U_\mu(x=n_x,y,z,t)$$

2.2.2 Plaquettes

The SU(2) group is defined by two factors. First, the determinant of the group element is unity (detU=1). Second, the elements U_μ are unitary ($UU^\dagger=1$). The group is closed under multiplication.

The smallest non-trivial object that can be built from the link operator U_μ is the so-called plaquette operator $U_{\mu\nu}$. The plaquette is the product of the link variables around the square starting at site x and in the $\mu\nu$ plane.

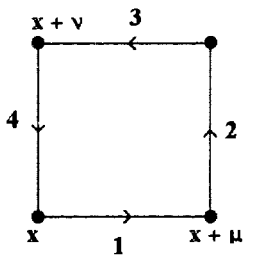

$$U_{\mu\nu}(x) = U_\mu(x)\, U_\nu(x+\hat{\mu})\, U_\mu^\dagger(x+\hat{\nu})\, U_\nu^\dagger(x) = U_1 U_2 U_3^\dagger U_4^\dagger$$

Figure 2.2 Plaquette on a lattice.

Initially consider a U(1) or Abelian lattice theory. Then using the definition

$$U_\mu(x) = e^{i\int_x^{x+a\hat{\mu}} gA_\mu(x')\,dx'} \approx e^{iagA_\mu(x)}$$

Doing the multiplication for the plaquette results in

$$\begin{aligned} U_{\mu\nu}(x) &= U_\mu(x)\, U_\nu(x+\hat{\mu})\, U_\mu^\dagger(x+\hat{\nu})\, U_\nu^\dagger(x) \\ &= e^{igaA_\mu(x)}\, e^{igaA_\nu(x+\hat{\mu})}\, e^{-igaA_\mu(x+\hat{\nu})}\, e^{-igaA_\nu(x)} \\ &= e^{iga[A_\nu(x+\hat{\mu}) - A_\nu(x) - A_\mu(x+\hat{\nu}) + A_\mu(x)]} \\ &\approx e^{iga[a\,\partial_\mu A_\nu(x) - a\,\partial_\nu A_\mu(x)]} \\ &= e^{iga^2 F_{\mu\nu}} \end{aligned}$$

and expanding in terms of the lattice spacing a the result is

$$U_{\mu\nu}(x) = \mathbb{I} + ia^2 gF_{\mu\nu} - \frac{a^4}{2!} g^2 F_{\mu\nu}^2 + \cdots$$

In Yang-Mills theory $F_{\mu\nu} = F_{\mu\nu}^b \frac{\sigma_b}{2}$ [21]. The Baker-Hausdorff theorem shows that for matrices

$$e^A e^B \approx e^{A + B - \frac{1}{2}[A,B]}$$

and therefore in SU(2)

$$F_{\mu\nu} = \partial_\mu A_\nu - \partial_\nu A_\mu + ig\left[A_\mu, A_\nu\right]$$

To complete the connection between lattice and continuum theories consider the action in the continuum Euclidian field theory given by

$$S = \frac{1}{4}\int d^4x\ F^{b}_{\mu\nu}F^{b}_{\mu\nu} = \frac{1}{2}\int d^4x\ Tr\left(F_{\mu\nu}F_{\mu\nu}\right)$$

This action is used in the Feynman path integral

$$\prod_x \prod_\mu \int \left[dA_\mu(x)\right] e^{-S}$$

In a similar way the lattice quantum theory is defined by a path integral over the link variables U_μ for the discrete lattice as

$$\prod_x \prod_\mu \int \left[dU_\mu(x)\right] e^{-S}$$

where in the conventional formulation due to Wilson the action is given by:

$$S = -\frac{\beta}{2}\sum_x\sum_{\mu,\nu} Tr\left(U\mu\nu\right)$$

This quantum theory leads to continuum QCD since in the continuum limit ($a \rightarrow 0$) $U_\mu(x) \approx 1 + iaA_\mu(x)$ and $\beta\frac{1}{2}Tr\,U_{\mu\nu} \approx \beta - \frac{a^4}{4}(F_{\mu\nu})^2$ where $\beta = 4/g^2$. This formalism gives the same results for observables as the continuum field theory Feynman path integral since the factor of e^β is normalized away.

2.2.3 Gauge Invariance

The research involves a non-Abelian gauge theory in SU(2) first proposed by Yang and Mills [21]. In this theory, the transformation law for A_μ is given by:

$$A_\mu(x) \rightarrow \Omega(x)A_\mu(x)\Omega^\dagger(x) - \frac{i}{g}\Omega(x)\partial_\mu\Omega^\dagger(x)$$

where $A_\mu \equiv A_\mu^b \frac{\sigma^b}{2}$ and $\Omega \equiv e^{i\omega^b \frac{\sigma^b}{2}}$. The first term in the transformation can be thought of as generating a rotation in an internal space ("colour space" or sometimes "isospace") while the second generates a "shift". Using the expression for $F_{\mu\nu}$ given in the last section the field strength tensor transforms as $F_{\mu\nu}(x) \rightarrow \Omega(x)F_{\mu\nu}(x)\Omega^\dagger(x)$ which is just a pure rotation. The trace of this quantity is gauge invariant.

This suggests that the link variable transformation law can be written as

$$U_\mu(x) \Rightarrow \Omega(x)\, U_\mu(x)\, \Omega^\dagger(x+\mu)$$

which incorporates the rotation and shift transformations of the A_μ (which lives in the group algebra while U_μ is an element of the group). Under this transformation the trace of the plaquette described in the last section is gauge invariant.

This also gives the recipe to test gauge invariance of the action on the lattice. One can easily apply $\Omega(x)\, U_\mu(x)\, \Omega^\dagger(x+\mu)$ to an entire SU(2) lattice by generating some local gauge transformations $\Omega(x)$ for each site in the same SU(2) group. Then gauge invariance is tested by comparing a gauge invariant observable such as plaquette value at each site on both the original and transformed lattice. For this thesis a sampling of all lattices generated in all simulations was specifically tested for gauge invariance to insure proper running of the computer programs.

As is clearly shown by $\Omega(x)\, U_\mu(x)\, \Omega^\dagger(x+\mu)$ the link variable transports the field from one end of the link to the other, similar to parallel transport.

2.3 Potential between Heavy Quarks

To study the interaction of heavy particles the gauge fields are allowed to fluctuate in the presence of a static charge density current. Therefore the action will require an interaction term and will become

$$S = \frac{1}{4} \int d^4x \; Tr\left(F_{\mu\nu} F_{\mu\nu} \right) - i \int d^4x \; Tr\left(J_\mu A_\mu \right)$$

where J_μ must satisfy current conservation. The Feynman path integral equivalent to solving the functional Schrödinger equation is the same as before

$$\prod_x \prod_\mu \int \left[dA_\mu(x) \right] e^{-S}$$

Now consider in an Abelian theory, a heavy "quark" at position x_1 with a static charge density $J^0 = Q\,\delta^3(\vec{x}_1)$. Then the interaction term of the Feynman path integral will become

$$e^{i \int d^4x \; J^\mu A^\mu} = e^{iQ \int dt \; A^0(\vec{x}_1, t)}$$

In terms of link variables this can be written as a Wilson line, the product of link variables along the time coordinate:

$$\prod_{t_i}^{t_f} U_0(\vec{x}_1, t)$$

An "anti-quark" at position x_2 with a static charge density $J^0 = -Q\,\delta^3(\vec{x}_2)$ will make a similar Wilson line but going the other way. To complete the current flow around a loop such

as in figures 2.3 and 2.4, there is a need for current conservation along the spatial edges which can also be expressed as Wilson lines. Taken together these lines form a Wilson loop.

Under SU(2), a "natural" generalization which preserves gauge invariance is the trace of a path ordered product. The next section deals with this in detail.

2.3.1 Wilson Loops

The heavy quark potential is measured using a quantity called a Wilson loop which is defined in the continuum as $W(C) = \mathrm{Tr}\ \underline{P}\ e^{-i\oint_C dx_\mu g A_\mu(x)}$ for some closed path C. As I will demonstrate, the analogous quantity on the discrete lattice is given by an ordered product of link variables. For example the discrete lattice Wilson loop for a 2x2 square is

$$W(C) = \frac{1}{2}\mathrm{Tr}\left(U_\mu(x)U_\mu(x+\hat{\mu})U_\nu(x+2\hat{\mu}) \cdots U_\nu^\dagger(x+\hat{\nu})U_\nu^\dagger(x)\right)$$

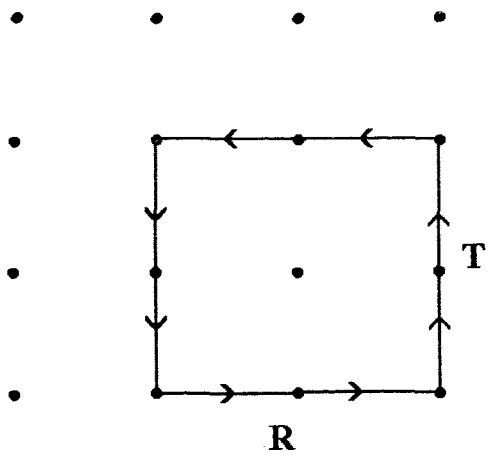

Figure 2.3 2x2 Wilson loop on the lattice.

Note that the smallest non-trivial Wilson loop on the lattice is the plaquette.

On the lattice the Wilson loop is normally denoted by W(R,T) where R is the

"spatial" direction and T is the"temporal" direction. R and T give the number of lattice spacings in the corresponding coordinate, for example the 2x2 square given above is W(2,2).

The following will demonstrate how the Wilson loops measure the interaction of a quark anti-quark pair. The derivation presented here is somewhat original as I could not find this derivation in the standard literature. The plan is to solve the Schrödinger equation for heavy particles. If there were no interactions this would be:

$$i\hbar\frac{\partial\psi}{\partial t} = \frac{P^2}{2m}\psi$$

For heavy particles, $m \to \infty$, and the right hand side will be zero. The gauge field interactions are included by making the substitution $\partial_t \to \partial_t - igA_a^0\frac{\sigma_a}{2}$ in SU(2). Setting $\hbar=1$, the Schrödinger equation for the interaction of a single heavy quark with a colour field is

$$i\frac{\partial\psi}{\partial t} = -gA_a^0\frac{\sigma_a}{2}\psi = H\psi$$

where H is the interaction Hamiltonian. The solution to the Schrödinger equation is

$$\psi(x,t) = T\left\{ e^{-i\int_0^t H(t')\,dt'} \right\}\psi(x,0)$$

where T is the time ordered product. A Taylor expansion of the exponential gives

$$\psi(x,t) = T\left\{ \sum_{n=0}^{\infty}\frac{1}{n!}\left(-i\int_0^t H(t')\,dt' \right)^n \right\}\psi(x,0)$$

Because H is composed of matrices, the order of factors in this Taylor expansion is important. This is accomplished by the time ordering operator T which ensures the proper

sequence of factors by putting all operators with later times on the left. Then the solution to the Schrödinger equation will be

$$\psi(x,t_f) = T\left(e^{-i\int_{t_i}^{t_f} H(t')\,dt'}\right)\psi(x,t_i) = T\left(e^{ig\int_{t_i}^{t_f} A_a^0(t')\frac{\sigma_a}{2}\,dt'}\right)\psi(x,t_i)$$

Consider a quark with initial colour (or "isospin") $|a\rangle$ and final isospin $\langle b|$ at position x_1. From the last equation, the amplitude that the quark makes such a transition can be written in terms of link variables as

$$\langle b|U_0(\vec{x}_1,t_f)\cdots U_0(\vec{x}_1,t_i)|a\rangle$$

The amplitude for an anti-quark at position x_2 can be written similarly. The intention is to measure the energy of a colour singlet state since confinement says there is infinite energy for a naked quark. This colour singlet is written as $\frac{1}{\sqrt{2}}\left(|\uparrow\rangle_Q|\downarrow\rangle_{\bar{Q}} - |\downarrow\rangle_Q|\uparrow\rangle_{\bar{Q}}\right)$ just as for ordinary spin. Then the amplitude for a transition from a colour singlet $Q\bar{Q}$ pair at time t_i to a colour singlet at time t_f is

$$\sum_{b=\pm}\frac{b}{\sqrt{2}}\sum_{a=\pm}\frac{a}{\sqrt{2}}\langle b|U(\vec{x}_1,t_f)\cdots U(\vec{x}_1,t_i)|a\rangle\langle -b|U(\vec{x}_2,t_f)\cdots U(\vec{x}_2,t_i)|-a\rangle$$

Notice the colour-singlet pairing of initial colours $|a\rangle$ with $|-a\rangle$ and final colours $\langle b|$ with $\langle -b|$.

Now consider the Pauli spin matrix σ_2. A feature of this matrix is its effect on spinors:

$$\sigma_2|+\rangle = \begin{pmatrix}0 & -i\\ i & 0\end{pmatrix}\begin{pmatrix}1\\0\end{pmatrix} = \begin{pmatrix}0\\i\end{pmatrix} = i|-\rangle$$

Similarly $\sigma_2|-\rangle = -i|+\rangle$ so that $\sigma_2|a\rangle = ia|-a\rangle$ and thus $-ia\sigma_2|a\rangle = |-a\rangle$ and $ib\langle b|\sigma_2 = \langle -b|$. Therefore the amplitude of the colour singlet transition is:

$$\sum_{b=\pm}\sum_{a=\pm}\frac{1}{2}\langle b|U(\vec{x}_1,t_f)\cdots U(\vec{x}_1,t_i)|a\rangle\langle b|\sigma_2 U(\vec{x}_2,t_f)\cdots U(\vec{x}_2,t_i)\sigma_2|a\rangle$$

The scheme is to drag the last σ_2 through to the first and cancel them out. For all σ, $\sigma\sigma_2 = -\sigma_2\sigma^*$ because each Pauli spin matrix anticommutes with all others and commutes with itself. Therefore dragging the last σ_2 through to the first will result in changing the sign of and conjugating all Pauli matrices pulled through. Then

$$U(\vec{x},t)\,\sigma_2 = T\left(e^{ig\int_0^t A_a^0(t')\frac{\sigma_a}{2}dt'}\right)\sigma_2 = \sigma_2 T\left(e^{-ig\int_0^t A_a^0(t')\frac{\sigma_a^*}{2}dt'}\right)$$

$$= \sigma_2 T\left(e^{ig\int_0^t A_a^0(t')\frac{\sigma_a}{2}dt'}\right)^* = \sigma_2 U(\vec{x},t)^*$$

Now the amplitude of the colour singlet transition is

$$\sum_{b=\pm}\sum_{a=\pm}\frac{1}{2}\langle b|U(\vec{x}_1,t_f)\cdots U(\vec{x}_1,t_i)|a\rangle\langle b|U(\vec{x}_2,t_f)^*\cdots U(\vec{x}_2,t_i)^*|a\rangle$$

Transposing the second bra-ket results in

$$\sum_{b=\pm}\sum_{a=\pm}\frac{1}{2}\langle b|U(\vec{x}_1,t_f)\cdots U(\vec{x}_1,t_i)|a\rangle\langle a|[U(\vec{x}_2,t_f)\cdots U(\vec{x}_2,t_i)]^{*T}|b\rangle$$

Combining the transpose and conjugation and removing the brackets gives

$$\sum_{b=\pm}\sum_{a=\pm}\frac{1}{2}\langle b|U(\vec{x}_1,t_f)\cdots U(\vec{x}_1,t_i)|a\rangle\langle a|U(\vec{x}_2,t_i)^\dagger\cdots U(\vec{x}_2,t_f)^\dagger|b\rangle$$

This is one half of a trace of the product of link variables and although it is the adjoint of the

two "temporal" lines in the Wilson loop it is still equivalent since $Tr(U) = Tr(U^{\dagger})$ in SU(2).

This equation is incomplete as it stands. To complete the Wilson loop, the requirement is to close the two "temporal" lines with "spatial" lines both top and bottom as shown in Figure 2.4.

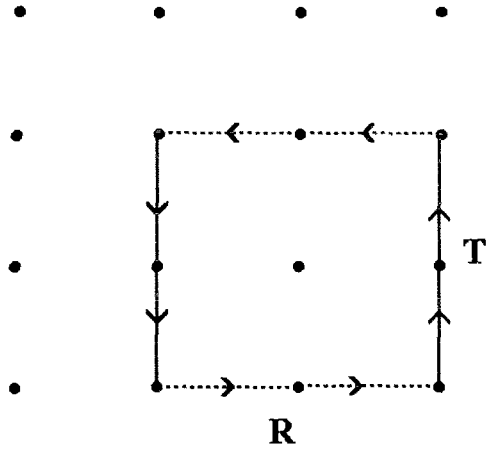

Figure 2.4 Wilson lines joined in a Wilson loop.

To understand why this is required, recognize that two wave functions at different "spatial" positions, for example $\psi(x)$ and $\psi(x+\varepsilon)$ are being compared. Due to the local gauge invariance of the theory, each of these wave functions can be independently changed by a local unitary operator to become $e^{i\theta(x)}\psi(x)$ and $e^{i\theta(x+\varepsilon)}\psi(x+\varepsilon)$ respectively. Since these matrix-valued phases are independent of each other, a direct comparison between $\psi(x)$ and $\psi(x+\varepsilon)$, such as a comparison of their SU(2) components (i.e. the quark colours), is meaningless. A comparator field $\Omega(x+\varepsilon,x)$ is used to compensate for the phase changes. (For a pedagogical review see, for example, reference [22].) This comparator field is defined so that it transforms under the local gauge transformation as $e^{i\theta(x+\varepsilon)}\Omega(x+\varepsilon,x)e^{-i\theta(x)}$. Therefore a comparison of $\psi(x+\varepsilon)$ with $\Omega(x+\varepsilon,x)\psi(x)$ is possible since they both transform in the same way. For instance a gauge-covariant derivative may be defined as:

$$D_{\hat{e}}\,\psi(x) = \lim_{\varepsilon \to 0} \frac{\psi(x+\varepsilon) - \Omega(x+\varepsilon,x)\,\psi(x)}{\varepsilon}$$

Then defining

$$\Omega(x+\varepsilon,x) \approx \mathbb{I} + i\varepsilon g A_{\varepsilon}(x)$$

in the limit of small ε results in the usual covariant derivative

$$D_{\hat{\varepsilon}} = \partial_{\hat{\varepsilon}} + igA_{\hat{\varepsilon}}$$

where the local gauge field has emerged.

To relate the comparator fields to the lattice link variables, postulate a composition rule (both sides transform in the same way): $\Omega(x_1+\varepsilon,x_2) = \Omega(x_1+\varepsilon,x_1)\,\Omega(x_1,x_2)$. Now evaluate a "spatial" derivative of $\Omega(x_1,x_2)$ and derive the following relationship

$$\frac{\partial\Omega(x_1,x_2)}{\partial x_1^{\,i}} = \lim_{\varepsilon \to 0} \frac{\Omega(x_1+\varepsilon,x_2) - \Omega(x_1,x_2)}{\varepsilon}$$

$$= \lim_{\varepsilon \to 0} \frac{(\Omega(x_1+\varepsilon,x_1) - \mathbb{I})\,\Omega(x_1,x_2)}{\varepsilon}$$

$$\equiv igA^{i}(x_1)\,\Omega(x_1,x_2)$$

where the local gauge field A^i has again appeared. Therefore

$$\Omega(x_1,x_2) = \underline{P}\; e^{\,ig\int_{x_1}^{x_2} A^{i}(x')\,dx'}$$

where $\underline{P}$ means path ordered product, analogous to the previous time ordered product. Thus the comparator field is a path ordered product and is used to ensure a gauge covariant

definition of a colour singlet $Q\bar{Q}$ state. The quarks are paired up in colour although separated and this comparator field will match up the phases. The comparator fields are laid out along the "spatial" lines of the Wilson loop. One comparator field is required at t_i and another at t_f to account for the phase changes in the initial and final quark wavefunctions. Note that the path from x_1 to x_2 is not unique, as evidenced by the composition rule. This fact will be used later in developing the fuzzing technique.

The comparator field completes the Wilson loop which is as I defined it at the beginning of this section. While the derivation of the Wilson loop has been non-relativistic, $W(C) = \mathrm{Tr}\ \underline{P}\ e^{-i\oint_C dx_\mu g A_\mu(x)}$ is in fact manifestly Lorentz invariant.

2.3.2 Static Quark Potential

The expectation value of the Wilson loop can be understood as

$$\langle W(R,T)\rangle = \langle f|e^{-HT}|i\rangle$$

where $\langle f|$ and $|i\rangle$ are the final and initial states which are composite states including quantum numbers for the quark and antiquark as well as gluons created by the comparator fields Ω. The final and initial states are not eigenstates of the interaction Hamiltonian. The introduction of a complete set of eigenvectors results in

$$\langle f|e^{-HT}|i\rangle = \langle f|e^{-HT}\left(\sum_n |n\rangle\langle n|\right)|i\rangle$$

$$= \sum_n e^{-\epsilon_n T}\langle f|n\rangle\langle n|i\rangle$$

Thus doing the path integral weighted by the Wilson loop gives the expectation value of the Wilson loop which will be a linear combination of exponentials of the energy spectrum:

$$\langle W(R,T)\rangle = a e^{-V(R)T} + b e^{-V_i(R)T} + \cdots$$

$$\equiv c e^{-V(R,T)T}$$

This last line defines a time-dependent estimate of potential. V(R,T) does not measure the energy of an actual eigenstate. Rather it is a convenient measure of the approach to V(R) in the $T \to \infty$ limit.

Potentials between quarks in other than their ground state will be larger than the ground state potential and thus will fall off at a faster rate in $\langle W(R,T)\rangle$. Then the potential energy between the two static quarks in their ground state can be calculated in the limit as T goes to infinity:

$$V(R) = \lim_{T\to\infty} -\ln \frac{\langle W(R,T)\rangle}{\langle W(R,T-1)\rangle}$$

$$= \lim_{T\to\infty} V(R,T)$$

2.3.3 Non-Integer Potentials

The method outlined in Section 2.3.2 for calculating static quark potentials can be used to calculate potentials that are not at exact integer lattice spacings by using a path where the "spatial" leg of the Wilson loop is taken along two or three dimensions. For example if the R leg is made by one lattice unit in the x direction and one lattice unit in the y direction then by Pythagoras' Theorem the result should correspond to a potential at a quark separation of $R = \sqrt{2}$. At least this should be true in the continuum limit where the lattice cubic symmetry should be restored to a continuum rotational symmetry. Similar methods will be used to get the square roots of five and eight using a 2x1 and 2x2 leg respectively. The square root of three requires the use of a "spatial" leg of one lattice unit in all three "spatial"

dimensions.

There is more than one path possible in these multi-dimensional "spatial" legs. For example the state with $\mathbf{R} = \sqrt{2}$ could be created along paths ⌋ or ⌐. The symmetric linear combination of paths ⌋ + ⌐ is used, as it has been demonstrated in the literature to correspond to the ground state.[23] One spatial path combination joins the lines along T at $T=t_i$ and another spatial path combination joins them at $T=t_f$.

For the 2x1 leg used in $\mathbf{R} = \sqrt{5}$ there are three paths from one corner to the other as shown in figure 2.5. Two are on the perimeter and one zigzags across. All three have been included symmetrically.

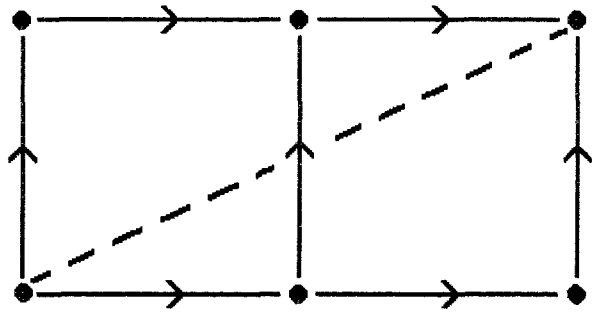

Figure 2.5 Example of off-axis potential. The dashed line shows $\mathbf{R} = \sqrt{5}$.

The 2x2 leg used in $\mathbf{R} = \sqrt{8}$ has four zigzag paths from one corner to the other plus two legs that follow the perimeter. The four zigzags are included symmetrically while the perimeter legs are dropped as they are getting quite far away from the central "direct' path and likely will be more strongly contaminated by finite lattice spacing errors.

The three dimensional leg used in $\mathbf{R} = \sqrt{3}$ has six unique paths from one corner of the cube to that opposite. All these are included symmetrically and required some very complicated computer logic to do this.

The off-axis potentials provide indicators of the approach to the continuum limit and

the restoration of rotational symmetry as discussed in more detail in Chapter 3. For example if a line is fitted to the on-axis (integer) potentials then the deviation of the off axis potentials from this line would quantify the breaking of rotational symmetry by the action used.

2.3.4 Lattice Spacing

The slope of the static potential between two heavy quarks is denoted in lattice units (a≡1) by m. It is related to the slope $\Delta V/\Delta R$ in physical units by the formula:

$$m = \frac{a\,V(R=n) - a\,V(R=m)}{\left(\frac{R}{a} = n\right) - \left(\frac{R}{a} = m\right)} = a^2 \frac{\Delta V}{\Delta R}$$

This quark potential is related to the string tension, σ, by

$$V(R) = \sigma R + \frac{1}{R} \quad \text{so} \quad \frac{\Delta V}{\Delta R} \approx \sigma \quad \text{at large R.}$$

Thus the lattice spacing is given by

$$a = \frac{\sqrt{m}}{\sqrt{\sigma}}$$

To get to physical units, the values used are $\sqrt{\sigma} \approx 0.44$ GeV and $\hbar c \approx 0.197$ GeV-fm. The value $\sqrt{\sigma} \approx 0.44\text{GeV}$ comes from an analysis of experimental data on light meson Regge trajectories using a simple string model for quark confinement. (For a pedagogical review see, for example, reference [24].) Although the experimental value should only be used for SU(3) colour simulations (with vacuum polarization), it is nevertheless used as the industry standard in SU(2) colour. For example see reference [20].

2.4 Statistical Simulations

Computing the expectation value of an observable in lattice QCD would require a very large number of integrations if conventional Riemann sum techniques are used. For example the expectation value of a Wilson loop is given by

$$\langle W \rangle = \frac{\int \left[dU_\mu \right] W(U_\mu)\, e^{-S(U_\mu)}}{\int \left[dU_\mu \right] e^{-S(U_\mu)}}$$

Using an 8^4 space-time lattice would give 4 x 8^4 link variables. In SU(2) each link variable is comprised of 3 parameters and therefore approximately 50,000 integrations need to be done. Using a Reimann sum with only 8 points per integration, the multiple integral would require a sum of $8^{50,000}$ terms. Therefore statistical methods are normally employed to make the problem tractable. The statistical technique used in this research is the Monte Carlo method.

2.4.1 Monte Carlo Simulations

In a Monte Carlo simulation a sequence of link variable configurations is generated by a stochastic process such that the probability of obtaining a certain configuration is given by the Boltzmann factor, $e^{-S(U_\mu)}$. In a simulation of N configurations the desired quantity, for example the value of a Wilson loop W_i, is calculated for each configuration. The expectation value of this Wilson loop is then given by

$$\langle W \rangle = \lim_{N \to \infty} \frac{1}{N} \sum_{i=1}^{N} W_i$$

The method that I used to generate the sequence of link variable configurations is

called the "heat-bath" method. In this method a link variable is replaced with a new value whose probability is given by a local Boltzmann distribution, with the rest of the link variables being fixed. The method is so named because in effect the link being updated is thermalized by touching it with a heat bath reservoir determined by the surrounding links. The local Boltzmann distribution is determined by the so-called "staples" connected to the link. Figure 2.6 shows two staples connected to a link variable. For a given link U_μ there are six staples, two for each perpendicular orientation. For an orientation μ, one staple is the product of the other three links which would make the plaquette $U_{\mu\nu}$. The other staple is from the plaquette formed by using $-\nu$ instead of ν.

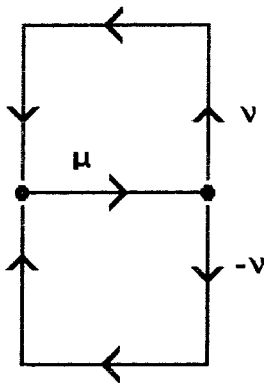

Figure 2.6 Staples connected to a lattice link variable.

The first step in generating the lattice link configurations is to get a configuration which satisfies the probability distribution. This was done by beginning with a cold lattice, where $U(4,\mu,x) = 1$ and $U(i,\mu,x) = 0$, $i=1,2,3$. Then the heat bath is applied iteratively to each configuration to make the next configuration. One iteration consists of applying the heat bath to one link at a time until all links have been updated. A sufficient number of iterations are applied until the lattice satisfies the Boltzmann distribution. At this point the lattice is said to be thermalized. In all of my simulations the initial cold starts were iterated through 10,000 configurations to achieve this equilibrium.

After thermalization a sequence of configurations is then generated to be used to measure the required observable. However, since each Monte Carlo step only causes a local change in the system, it requires a number of configurations to be generated until the memory of a previous configuration has decayed away, making the resulting link variables independent of this previous configuration. This phenomenon is known as relaxation and one can associate a correlation time with this decay. Typically in the case of critical phenomena the correlation time scales inversely as the second power of the lattice spacing, $1/a^2$. In the simulations every n'th configuration generated was used for measurement. The value of n was determined so as to minimize the auto-correlations between configurations used in measurement.

2.4.2 Error Determination

If the sequence of configurations used in measurement constitutes a representative set then the ensemble average of an observable such as the Wilson loop will be approximated by

$$\langle W \rangle \approx \frac{1}{N} \sum_{i=1}^{N} W_i$$

By ensuring that the N measurements are statistically independent by the procedure outlined in the last section, the statistical error in the expectation value will be of the order $1/\sqrt{N}$. The statistical error, σ, in the average of some observable is given by $\sigma = \sqrt{\langle x^2 \rangle - \langle x \rangle^2} \; / \; \sqrt{N-1}$.

For a derived quantity like the logarithm of the Wilson loop, we must "propagate" the errors. An efficient algorithm for doing this is the Jackknife method.[25] Using the static quark potential as an example, the first step is to calculate the average V(R) from all configurations (N) used for measurement. Next is to calculate V(R) for all the configurations

less one (N-1) which I will denote as $V_j(R)$, j indicating the configuration skipped. This last step is repeated saving a new $V_j(R)$ for each missed configuration. The error is then calculated as

$$\sigma_V = \sqrt{\sum_j \left(V(R) - V_j(R) \right)^2 \left(1 - \frac{1}{N} \right)}$$

This method is equivalent to the statistical error quoted earlier when V(R) is a simple average. For derived quantities, the Jackknife has become a lattice industry standard.

Chapter 3

Tadpole Improvement

Over the years, researchers have determined that a good approximation to the continuum limit can be achieved for a variety of observables with lattice spacings in the range of about 0.05 fm to 0.1 fm. For examples, see references [3], [20] and [26]. In moving from the continuum to the lattice, discretization approximations have been introduced. The expectation is that these approximations will introduce errors that are of leading order $(a/r_0)^2$, where r_0 is a characteristic dimension of the observable under consideration. Thus the smaller the lattice spacing, the smaller the errors. Attempts have been made in the past to remove the leading discretization errors [27], [28] which I will discuss under the classical improvement section. These improvements did not remove all $O(a^2)$ errors due to the quantum effects [4] which have only recently been understood. This I will discuss under the tadpole improvement section. The effect of tadpole improvement should be to remove all leading $O(a^2)$ errors and thus allow the use of larger lattice spacing with results potentially as accurate as those achieved using smaller lattice spacings.

3.1 Classical Improvement

In the mid 1980's a technique was developed to remove the leading discretization errors from lattice field theory. [27] [28] The complete derivation is not published and so is developed here for the convenience of the reader. Initially consider a U(1) or Abelian lattice theory.

Take a plaquette such as the one at the right with lattice spacing a and centred at x_c. The plaquette is a path integral in the $\mu\nu$ plane written as $U_{\mu\nu} = e^{ig\oint A_{\mu'} dx_{\mu'}}$ (sum over μ') and can be related to the surface area according to Stokes Theorem by $U_{\mu\nu} = e^{ig\int_s F_{\mu\nu} dx_\mu dx_\nu}$ (no sum on μ,ν). A Taylor expansion of $F_{\mu\nu}$ about x_c gives (again no sum on μ,ν)

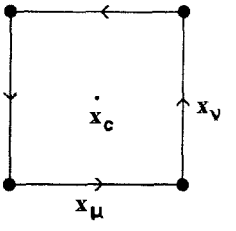

$$F_{\mu\nu}(x) = F_{\mu\nu}(x_c) + \partial_\mu F_{\mu\nu}(x_c)\,(x_\mu - x_c) + \partial_\nu F_{\mu\nu}(x_c)\,(x_\nu - x_c)$$
$$+ \frac{1}{2!}\,\partial_\mu^2 F_{\mu\nu}(x_c)\,(x_\mu - x_c)^2 + \frac{1}{2!}\,\partial_\nu^2 F_{\mu\nu}(x_c)\,(x_\nu - x_c)^2$$
$$+ \frac{1}{2!}\,\partial_\mu\partial_\nu F_{\mu\nu}(x_c)\,(x_\mu - x_c)(x_\nu - x_c) + \cdots$$

I define $x_c = 0$ to keep the mathematics from being too cluttered and hard to follow. Doing the integral from -a/2 to +a/2 the terms odd in x_μ and x_ν vanish and to first order the result is

$$\int_s F_{\mu\nu} dx_\mu dx_\nu = F_{\mu\nu} \int_{-\frac{a}{2}}^{+\frac{a}{2}} dx_\mu \int_{-\frac{a}{2}}^{+\frac{a}{2}} dx_\nu + \frac{1}{2}\partial_\mu^2 F_{\mu\nu} \int_{-\frac{a}{2}}^{+\frac{a}{2}} x_\mu^2 dx_\mu \int_{-\frac{a}{2}}^{+\frac{a}{2}} dx_\nu + \frac{1}{2}\partial_\mu^2 F_{\mu\nu} \int_{-\frac{a}{2}}^{+\frac{a}{2}} dx_\mu \int_{-\frac{a}{2}}^{+\frac{a}{2}} x_\nu^2 dx_\nu$$

$$= a^2 F_{\mu\nu} + \frac{1}{24}\, a^4 (\partial_\mu^2 + \partial_\nu^2) F_{\mu\nu} + O(a^6)$$

For ease of notation label this result as $\theta(1x1)$

$$\theta(1x1) \equiv \int_s F_{\mu\nu} dx_\mu dx_\nu = a^2 F_{\mu\nu} + \frac{1}{24} a^4 (\partial_\mu^2 + \partial_\nu^2) F_{\mu\nu} + O(a^6)$$

The Wilson action in the Abelian theory is defined by

$$S_W[U_{\mu\nu}] = \frac{\beta}{2} \sum_{x,\mu\nu} \left(1 - \mathrm{Re} U_{\mu\nu} \right)$$

and in the continuum limit becomes

$$S_W \approx \frac{1}{4} \sum_{x,\mu\nu} \left(\theta^2(1x1) - \frac{1}{6} g^2 \theta^4(1x1) + \cdots \right)$$

(the odd terms being accompanied by an "i"). Now θ^2 contains terms of $O(a^4,a^6,a^8)$ while θ^4 contains terms of $O(a^8)$ and higher and can be dropped to leading and next-to-leading order in a. The integral $\int d^4x$ becomes a sum $\sum a^4$ and so the term of interest is $1/a^4\, \theta^2(1x1)$.

$$\frac{1}{a^4} \theta^2(1x1) = F_{\mu\nu}^2 + \frac{1}{12} a^2 F_{\mu\nu} (\partial_\mu^2 + \partial_\nu^2) F_{\mu\nu} + O(a^4)$$

Therefore the continuum action $\frac{1}{4} \int d^4x \, F_{\mu\nu}^2$ is recovered in the limit $a \to 0$. The leading discretization term has also been isolated in the action:

$$S_W = \frac{1}{4} \int d^4x \sum_{\mu,\nu} \left(F_{\mu\nu}^2 + \frac{1}{12} a^2 F_{\mu\nu} (\partial_\mu^2 + \partial_\nu^2) F_{\mu\nu} \right)$$

In the Wilson action this last term breaks the rotational invariance of the Euclidean theory. As described in section 2.3.3 the expectation is that the off-axis potentials would not be consistent with an extrapolation through the on-axis points. My simulations show this

point in section 7.3.

The plan now is to get rid of these a^2 errors by adding extra terms to the action. The idea is to use a linear combination of $\theta(1x1)$ and larger lattice structures like the one to the right. This specific rectangle I label $\theta_R(2x1)$ where the R refers to the extra piece being to the right. Doing the integral for $\theta_R(2x1)$ from - a/2 to + 3a/2 in the μ direction and from - a/2 to + a/2 in the ν direction, the even terms give

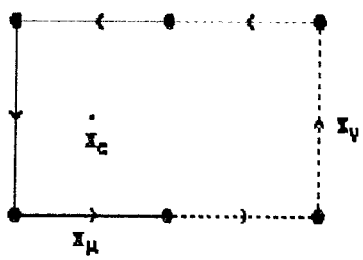

$$\int_s F_{\mu\nu}\,dx_\mu\,dx_\nu\Big|_{even} = F_{\mu\nu}\int_{-\frac{a}{2}}^{+3\frac{a}{2}} dx_\mu \int_{-\frac{a}{2}}^{+\frac{a}{2}} dx_\nu + \frac{1}{2}\partial_\mu^2 F_{\mu\nu}\int_{-\frac{a}{2}}^{+3\frac{a}{2}} x_\mu^2\,dx_\mu \int_{-\frac{a}{2}}^{+\frac{a}{2}} dx_\nu + \frac{1}{2}\partial_\mu^2 F_{\mu\nu}\int_{-\frac{a}{2}}^{+3\frac{a}{2}} dx_\mu \int_{-\frac{a}{2}}^{+\frac{a}{2}} x_\nu^2\,dx_\nu$$

$$= 2a^2 F_{\mu\nu} + \frac{7}{12}\,a^4\partial_\mu^2 F_{\mu\nu} + \frac{1}{12}\,a^4\partial_\nu^2 F_{\mu\nu}$$

In this case, not all the odd terms will vanish as in the case of $\theta(1x1)$, and to first order the odd terms are

$$\int_s F_{\mu\nu}\,dx_\mu\,dx_\nu\Big|_{odd} = \partial_\mu F_{\mu\nu}\int_{-\frac{a}{2}}^{+3\frac{a}{2}} x_\mu\,dx_\mu \int_{-\frac{a}{2}}^{+\frac{a}{2}} dx_\nu + \partial_\mu F_{\mu\nu}\int_{-\frac{a}{2}}^{+3\frac{a}{2}} dx_\mu \int_{-\frac{a}{2}}^{+\frac{a}{2}} x_\nu\,dx_\nu + \partial_\mu\partial_\nu F_{\mu\nu}\int_{-\frac{a}{2}}^{+3\frac{a}{2}} x_\mu\,dx_\mu \int_{-\frac{a}{2}}^{+\frac{a}{2}} x_\nu\,dx_\nu$$

$$= a^3\partial_\mu F_{\mu\nu}$$

Then $\theta_R(2x1)$ is

$$\theta_R(2x1) = 2a^2 F_{\mu\nu}^2 + a^3\partial_\mu F_{\mu\nu} + \frac{7}{12}\,a^4\partial_\mu^2 F_{\mu\nu} + \frac{1}{12}\,a^4\partial_\nu^2 F_{\mu\nu}$$

and $1/a^4\ \theta_R^2(2x1)$ is:

$$\frac{1}{a^4}\theta_R^2(2x1) = 4F_{\mu\nu}^2 + 4aF_{\mu\nu}\partial_\mu F_{\mu\nu} + \frac{7}{3}a^2F_{\mu\nu}\partial_\mu^2 F_{\mu\nu} + \frac{1}{3}a^2F_{\mu\nu}\partial_\nu^2 F_{\mu\nu}$$

$$+ a^2(\partial_\mu F_{\mu\nu})^2 + \frac{7}{6}a^3\partial_\mu F_{\mu\nu}\partial_\mu^2 F_{\mu\nu} + \frac{1}{6}a^3\partial_\mu F_{\mu\nu}\partial_\nu^2 F_{\mu\nu} + O(a^4)$$

Doing an integration by parts on the $a^2(\partial_\mu F_{\mu\nu})$ term results in

$$(\partial_\mu F_{\mu\nu})^2 = (\partial_\mu F_{\mu\nu})(\partial_\mu F_{\mu\nu}) = \partial_\mu(F_{\mu\nu}\partial_\mu F_{\mu\nu}) - F_{\mu\nu}\partial_\mu^2 F_{\mu\nu}$$

where $\partial_\mu(F_{\mu\nu}\partial_\mu F_{\mu\nu})$ is a total derivative which vanishes under integration due to periodic boundary conditions. Then finally $1/a^4\ \theta_R^2(2x1)$ is equivalent to

$$\frac{1}{a^4}\theta_R^2(2x1) = 4F_{\mu\nu}^2 + 4aF_{\mu\nu}\partial_\mu F_{\mu\nu} + \frac{4}{3}a^2F_{\mu\nu}\partial_\mu^2 F_{\mu\nu} + \frac{1}{3}a^2F_{\mu\nu}\partial_\nu^2 F_{\mu\nu}$$

$$+ \frac{7}{6}a^3\partial_\mu F_{\mu\nu}\partial_\mu^2 F_{\mu\nu} + \frac{1}{6}a^3\partial_\mu F_{\mu\nu}\partial_\nu^2 F_{\mu\nu} + O(a^4)$$

There are three other rectangles that are of interest. Namely the 2x1 rectangle to the left of the centre, the 1x2 rectangle to the top and the 1x2 rectangle to the bottom. By symmetry the left rectangle $1/a^4\ \theta_L^2(2x1)$ is the same as $1/a^4\ \theta_R^2(2x1)$ with the terms odd in μ changing sign. Similarly the bottom rectangle is the same as the top with terms odd in ν changing sign. This top rectangle is

$$\frac{1}{a^4}\theta_T^2(1x2) = 4F_{\mu\nu}^2 + 4aF_{\mu\nu}\partial_\nu F_{\mu\nu} + \frac{1}{3}a^2F_{\mu\nu}\partial_\mu^2 F_{\mu\nu} + \frac{4}{3}a^2F_{\mu\nu}\partial_\nu^2 F_{\mu\nu}$$

$$+ \frac{1}{6}a^3\partial_\nu F_{\mu\nu}\partial_\mu^2 F_{\mu\nu} + \frac{7}{6}a^3\partial_\nu F_{\mu\nu}\partial_\nu^2 F_{\mu\nu} + O(a^4)$$

Label a rectangle by the coordinate x of the lower left corner. Then the 1x2 rectangle

to the left of x is the same as the 1x2 rectangle to the right of the point x - μ. These two rectangles will automatically be included in $\sum_x \theta_R^2(x)$. Therefore the adjustments to a particular 1x1 plaquette can be associated with only two of the rectangles, while the other two will be associated with other 1x1 plaquettes. The adjustments for a plaquette are arbitrarily chosen to be the right and top rectangles. However, when summing over the entire lattice there will be a cancellation of the odd terms between $1/a^4\ \theta_R^2(2x1)$ and $1/a^4\ \theta_L^2(2x1)$ and between $1/a^4\ \theta_T^2(1x2)$ and $1/a^4\ \theta_B^2(1x2)$.

Therefore adding only the even terms of $1/a^4\ \theta_R^2(2x1)$ and $1/a^4\ \theta_T^2(1x2)$

$$\frac{1}{a^4}\left(\theta_R^2(2x1) + \theta_T^2(1x2) \right)\Big|_{even} = 8F_{\mu\nu}^2 + \frac{5}{3}a^2 F_{\mu\nu}(\partial_\mu^2+\partial_\nu^2)F_{\mu\nu} + O(a^4)$$

We finally return to the Wilson action, which contains $\theta^2(1x1)$ to $O(a^8)$. By subtracting 1/20 of the above equation the $O(a^6)$ errors are eliminated. The result is

$$\frac{1}{a^4}\left(\theta^2(1x1) - \frac{1}{20}\left(\theta_R^2(2x1) + \theta_T^2(1x2) \right) \right) = \left(1 - \frac{8}{20}\right)F_{\mu\nu}^2 + O(a^4)$$

$$= \frac{3}{5}F_{\mu\nu}^2 + O(a^4)$$

Back in section 2.2.2 I wrote the Wilson action for SU(2) as

$$S_W = -\frac{\beta}{2}\sum_x\sum_{\mu,\nu} \mathrm{Tr}\left(U_{\mu\nu} \right)$$

Using a slightly different notation where $P_{\mu\nu} = \frac{1}{2}\mathrm{Tr}U_{\mu\nu}$ this action can be written as

$$S_W = -\beta\sum_x\sum_{\mu,\nu} P_{\mu\nu}$$

As a consequence of these corrections an improved SU(2) action which is corrected up to $O(a^4)$ is proposed as

$$S_{imp} = -\beta \sum_{x} \sum_{\mu,\nu} \left(\frac{5}{3} P_{\mu\nu} - \frac{1}{12} R_{\mu\nu} - \frac{1}{12} R_{\nu\mu} \right)$$

$$= \int d^4x \, F_{\mu\nu}^2 + O(a^4)$$

where $R_{\mu\nu}$ is the 2x1 rectangle widest in the direction of the first subscript, in this case μ.

Actually the derivation has been done in an Abelian or U(1) lattice theory. This can be generalized to a non-Abelian theory by observing that the action is gauge invariant. For example, by dimensional analysis, the expectation is that a term such as $a^6 F_{\mu\nu} \partial_\mu F_{\mu\nu}$, in the expansion of dimensionless $P_{\mu\nu}$ or $R_{\mu\nu}$ in U(1), would become $a^6 F_{\mu\nu}^a D_\mu^{ab} F_{\mu\nu}^b$ where the covariant derivative is $D_\mu^{ab} = \partial_\mu \delta^{ab} + f^{abc} A^c$. Other gauge invariant bilinears on $F_{\mu\nu}$ would involve higher order derivatives and therefore be of higher order in a. In this way it is seen that S_{imp} should be $O(a^4)$ accurate in SU(2).

3.2 Tadpole Improvement

The classical improvement of the last section was developed in the mid 1980's.[27] [28]. However researchers who tried this improved action found that while discretization errors were reduced the improvement in many cases was not as significant as would be expected from the analysis of the classical improvement in the last section. The resolution of this problem was arrived at only recently by Lepage and Mackenzie [4]. The key lies in the fact that a classical field theory analysis was used in the last section.

To see this, consider an expansion of the link variable in terms of the lattice spacing:

$$U_\mu(x) = e^{i\int_x^{x+a\hat{\mu}} gA_\mu(x')\,dx'}$$

$$\approx e^{iagA_\mu(x)}$$

$$= 1 + iagA_\mu(x) - \frac{1}{2!}a^2g^2A_\mu^2(x) + \cdots$$

In quantum theory this last term induces what are called tadpole diagrams. For example, compute the expectation value of a link $\langle U_\mu(x)\rangle$. In lattice theory the expectation value of a gauge non-invariant quantity vanishes by Elitzur's theorem as described later in this section. So the evaluation of the expectation value must have a constraint that picks only one configuration out of the gauge equivalent set $\{\Omega U \Omega^\dagger\}$. The details of this gauge fixing are unimportant in this analysis. Using the above expansion

$$\langle U_\mu(x)\rangle_{gf} = \mathbb{I} + iag\langle A_\mu(x)\rangle_{gf} - \frac{1}{2}a^2g^2\langle A_\mu(x)^2\rangle_{gf} + O(a^3g^3)$$

In perturbation theory, the last term can be expressed in terms of a Feynman diagram called a tadpole. $\langle A_\mu(x)\rangle_{gf}$ vanishes under the trace.

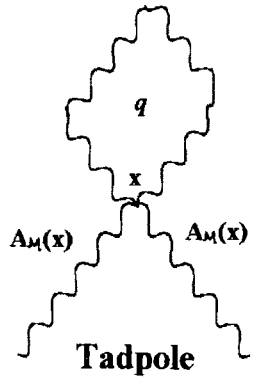

Figure 3.1 Feynman diagram of a tadpole.

The virtual gluon propagates in a closed loop with an amplitude $\propto 1/q^2$. Since all

virtual momenta are allowed, integrate over all possible values $\int d^4q \ \frac{1}{q^2}$. In the continuum this integral diverges. However on a lattice the integral runs over the first Brillouin zone with limits $\int_{-\Pi/a}^{\Pi/a}$. Therefore this tadpole is proportional to $1/a^2$ which means that in an expectation value A_μ has parts proportional to $1/a$ which cancel the explicit factor of a in $U_\mu \approx e^{iagA_\mu}$. The tadpole terms are suppressed by only g^2 and not by g^2a^2 as expected in a classical field theory analysis.

To get rid of the tadpoles one does a "tadpole improvement" of the action. Such improvement is defined by a mean field renormalization of the links. Defining the average link as U_0, the mean field renormalization is

$$U_\mu' = \frac{U_\mu}{U_0}$$

An obvious definition of the average link is $\langle U_\mu(x) \rangle \equiv U_0$. This definition of U_0 is not any good since $\langle U_\mu(x) \rangle = 0$ due to gauge invariance. This statement is formalized in Elitzur's Theorem [29] as demonstrated here. The gauge transformation of a lattice link is $U_\mu'(x) = \Omega(x) U_\mu(x) \Omega^\dagger(x+\hat{\mu})$. The expectation value of the lattice link is calculated by the Feynman path integral $\int [dU] \ e^{-S} \ U_\mu(x)$. Both U_μ' and U_μ will be found in the ensemble with exactly equal probability. Therefore in doing the integral on the discrete lattice a term $U_\mu(x_0) + \Omega(x_0) U_\mu(x_0) \Omega^\dagger(x_0+\hat{\mu})$ will occur, where x_0 is a particular value of x. A valid gauge transformation is one where $\Omega(x_0) = -\mathbb{I}$ and $\Omega(x \neq x_0) = \mathbb{I}$. This gauge transformation will make this term and therefore all terms vanish.

A definition of U_0 from a mean link could be made by gauge-fixing when computing $\langle U_\mu(x) \rangle$ although its value would not be unique (a proposal to use a smooth gauge such as $\partial_\mu A_\mu = 0$ has recently been made [30]). However a simpler alternative is to give a definition of the average link in terms of the smallest gauge invariant object which has a non-trivial value. The smallest object is a lattice line out and back. This is no good since

$U_\mu U_\mu^\dagger = 1$. The next smallest gauge invariant object is the average plaquette. The definition of U_0 is therefore given as

$$\langle U_{\mu\nu}(x) \rangle \equiv U_0^4$$

since there are four lattice links in the plaquette.

Now consider the expectation value of a gauge-invariant observable, such as a 2x2 Wilson loop $\langle W(2,2) \rangle$ which in an Abelian theory has the value $\left\langle e^{\int_{2x2} F_{\mu\nu} dx_\mu dx_\nu} \right\rangle$. Following the classical improvement analysis this has a continuum limit of

$$\langle W(2,2) \rangle \approx \mathbb{I} + 4a^4 g^2 \langle F_{\mu\nu}^2 \rangle + \frac{1}{3} a^6 g^3 \langle F_{\mu\nu} (\partial_\mu^2 + \partial_\nu^2) F_{\mu\nu} \rangle + O(a^8)$$

However each expectation value receives a tadpole contribution, which cancels the explicit factor of the lattice spacing. This spoils the expansion in powers of a that underlies the classical field theory analysis of the previous section.

The tadpole contribution to any observable such as $\langle W \rangle$ comes from very short distance physics (ultraviolet) and should be independent of the long distance physics (infrared). The continuum gauge field should have parts $A_\mu(x) = A_\mu(x)|_{I.R.} + A_\mu(x)|_{U.V.}$. This suggests that the link variable could be factored as $U_\mu(x) = U_\mu(x)|_{I.R.} \times U_\mu(x)|_{U.V.}$. The average value of this last factor is the average link U_0 since the plaquette occupies the smallest cell on the lattice (i.e. $U_0 = \langle U_\mu(x)|_{U.V.} \rangle$). Therefore tadpoles should be removed from the expectation value of an operator by first renormalizing the lattice links.

$$U_\mu'(x) = \frac{U_\mu(x)}{U_0} = U_\mu(x)|_{I.R.}$$

where the corrections are truly of higher order in a^2g^2 and not just g.

In developing the action from the lattice replace U_μ with U'_μ. This is called a tadpole-improved action. In the last section the classically improved action was:

$$S_{imp} = -\beta \sum_{x} \sum_{\mu,\nu} \left(\frac{5}{3} P_{\mu\nu} - \frac{1}{12} R_{\mu\nu} - \frac{1}{12} R_{\nu\mu} \right)$$

where $P_{\mu\nu}$ contains the product of four U_μ's and $R_{\mu\nu}$ contains the product of six U_μ's. Then the tadpole improved action is

$$S_{tad} = -\beta \sum_{x} \sum_{\mu,\nu} \left(\frac{5}{3} \frac{P_{\mu\nu}}{U_0^4} - \frac{1}{12} \frac{R_{\mu\nu}}{U_0^6} - \frac{1}{12} \frac{R_{\nu\mu}}{U_0^6} \right)$$

This action features a new kind of non-linearity, because U_0 must be determined from the average plaquette, which itself is determined by the value of U_0.

A final comment about discretization errors in S_{tad}. The classical field theory analysis, together with tadpole renormalization, suggests that $S_{tad} = S_{continuum} + O(a^4)$. In fact, each operator in S_{tad} gets additional renormalizations due to quantum effects. These effects spoil the cancellations of the $O(a^2)$ errors, but such corrections are suppressed by $g^2(a)$, the running coupling evaluated at a length scale of O(a). Therefore the leading discretization errors are actually of $O(a^2 g(a))$, plus errors of $O(a^4)$. For sufficiently small lattice spacing a, $g(a) \ll 1$. In fact $g(a) \propto 1/\ln(a)$. [31] On coarse lattices there is evidence that these two types of errors are actually comparable (and small). [4]

Chapter 4

Anisotropic Lattice

A significant feature of this thesis is the use of an anisotropic lattice. One coordinate is designated as the "temporal" coordinate with a lattice spacing denoted by a_t which is made smaller than the lattice spacing for the other three coordinates designated as "spatial" coordinates. The "spatial" lattice spacing a_s is chosen in the range of 0.2 fm to 0.4 fm. The "temporal" lattice spacing a_t is kept around 0.1 fm.

The use of anisotropic lattices allows one to more easily determine the glueball mass. The correlation function is $G(t) \rightarrow G_0 e^{-m_g t}$ as $t \rightarrow \infty$. This signal falls off rapidly with t while the noise in the Monte Carlo simulation remains fairly constant with t. The use of the anisotropic lattice allows one to get more measurements of this correlation function before it disappears into the noise.

4.1 Anisotropic Action

This research work is based upon an anisotropic lattice where all "spatial" lattice spacings a_s are the same and the "temporal" lattice spacing a_t is smaller. As a result there will be two values for the average link. One value is for plaquettes where both directions are "spatial".

The other value is where one direction is "spatial" and one is "temporal". These average links are defined as $\langle U_{ss}(x)\rangle \equiv U_{0s}^4$ and $\langle U_{st}(x)\rangle \equiv U_{0s}^2 U_{0t}^2$. The tadpole-improved action is then adjusted so that the mean field renormalization of the plaquettes includes the appropriate number of factors of U_{0s} and U_{0t}. The action will also require adjustments in the discrete integrals (sums) to account for the anisotropy. This action can be written as [16]:

$$S = -\beta \sum_x \sum_{s>s'} \frac{a_t}{a_s} \left\{ \frac{5}{3} \frac{P_{ss'}}{U_{0s}^4} - \frac{1}{12} \frac{R_{ss'}}{U_{0s}^6} - \frac{1}{12} \frac{R_{s's}}{U_{0s}^6} \right\}$$

$$-\beta \sum_x \sum_s \frac{a_s}{a_t} \left\{ \frac{4}{3} \frac{P_{st}}{U_{0s}^2 U_{0t}^2} - \frac{1}{12} \frac{R_{st}}{U_{0s}^4 U_{0t}^2} \right\}$$

Two explanations are required and will be given for this action. The first is for the a_t/a_s and a_s/a_t factors. The second is for the 4/3 factor and lack of an R_{ts} term in the mixed "spatial"/"temporal" portion.

The a_t/a_s and a_s/a_t terms are adjustments in the discrete integrals. The discrete integral for an isotropic lattice is given by $\int d^4x = \sum a^4$. This isotropic integral worked out fine in using the symmetric lattice to define the action since $P_{\mu\nu} = \frac{1}{2} \mathrm{Tr}\, U_{\mu\nu} \sim \frac{1}{4} a^4 (F_{\mu\nu})^2$. However for the anisotropic lattice this integral has to account for the different lengths of "spatial" and "temporal" coordinates and therefore becomes $\int d^4x = \sum a_s^3 a_t$. For the "spatial" plaquette $P_{ss} = \frac{1}{2} \mathrm{Tr}\, U_{ss} \sim \frac{1}{4} a_s^4 (F_{ss})^2$. Multiplication by a_t/a_s will adjust this result to get the correct integral . Similarly for the mixed "spatial"/"temporal" plaquette $P_{st} = \frac{1}{2} \mathrm{Tr}\, U_{st} \sim \frac{1}{4} a_s^2 a_t^2 (F_{st})^2$ and has to be multiplied by a_s/a_t for the integral to work properly.

The R_{ts} rectangles (with two spacings along a_0) have purposely been omitted from this action. Thus errors of the order a_t^2 have been introduced. These errors will be negligible provided that a_t is small compared to a_s.

The reason for dropping the R_{ts} term is to eliminate poles in the gluon propagator that have negative residues. [16] Due to the negative residue poles (called high-energy doublers) the correlation function does not decrease monotonically with time. Instead it shows a hump at intermediate times T, caused by the change in slope because of the negative residue. Eventually the correlation function decreases exponentially with the energy of a physical pole as the doublers can be shown to have very high energy $\propto 1/a_t$. This complicates the extraction of a plateau in the correlation function on an improved lattice.

Following the procedure of classical improvement (Section 3.1) I will derive this mixed "spatial"/"temporal" portion of the action, the details of which have not been published anywhere. On the anisotropic lattice the integration for $\theta(1x1)$ is from $-a_s/2$ to $a_s/2$ in the "spatial" direction and from $-a_t/2$ to $a_t/2$ in the "temporal" direction. As a result for a mixed plaquette

$$\theta_{st}(1x1) = a_s a_t F_{st} + \frac{1}{24} a_s^3 a_t \partial_s^2 F_{st} + \frac{1}{24} a_s a_t^3 \partial_s^2 F_{st}$$

Instead of $1/a^4\ \theta^2(1x1)$ use $1/(a_s^2 a_t^2)\ \theta_{st}^2(1x1)$ and drop terms in a^4

$$\frac{1}{a_s^2 a_t^2}\theta_{st}^2(1x1) = F_{st}^2 + \frac{1}{12} a_s^2 F_{st} \partial_s^2 F_{st} + \frac{1}{12} a_t^2 F_{st} \partial_t^2 F_{st} + O(a^4)$$

The final term of interest is $1/(a_s^2 a_t^2)\ \theta_{Rst}^2(2x1)$ since $1/(a_s^2 a_t^2)\ \theta_{Tst}^2(1x2)$ has two lattice links in the "temporal" direction and is therefore omitted. Dropping terms in a^4 and higher and also dropping terms that cancel with $1/(a_s^2 a_t^2)\ \theta_{Lst}^2(2x1)$ this expression is

$$\frac{1}{a_s^2 a_t^2}\theta_{Rst}^2(2x1) = 4F_{st}^2 + \frac{4}{3} a_s^2 F_{st} \partial_s^2 F_{st} + \frac{1}{3} a_t^2 F_{st} \partial_t^2 F_{st} + O(a^4)$$

Therefore to cancel out the a_s^2 corrections to $1/(a_s^2 a_t^2)\ \theta_{st}^2(1x1)$ subtract 1/16 of

$1/(a_s^2 a_t^2)$ $\theta_{Rst}^2(2x1)$. This gives a result of

$$\frac{1}{a_s^2 a_t^2}\left(\theta_{st}^2(1x1) - \frac{1}{16}\theta_{Rst}^2(2x1) \right) = \left(1 - \frac{4}{16}\right)F_{st}^2 + \frac{1}{16}a_t^2 F_{st}\partial_t^2 F_{st} + O(a^4)$$

$$= \frac{3}{4}F_{st}^2 + O(a_t^2) + O(a_s^4)$$

The plaquette trace of the mixed "spatial"/"temporal" portion of the action therefore has a factor 4/3. Errors of the order a_t^2 have been introduced. These errors will be negligible compared to the a_s^4 provided that a_t is small compared to a_s.

4.2 Set $U_{0t} = 1$

In this thesis I have set U_{0t} =1 and have determined U_{0s} self-consistently from the average value of the "spatial" plaquette for the entire ensemble:

$$U_{0t} = 1$$

$$U_{0s} = \langle P_{ss'} \rangle^{1/4}$$

The anisotropic action has an invariance under a rescaling of β, U_{0t} and a_t/a_s, which allows U_{0t} to be set to any value leaving the physical quantities invariant. That is equate:

$$\beta_{old}\left(\frac{a_s}{a_t}\right)_{old}\frac{1}{U_{0t}^2} = \beta_{new}\left(\frac{a_s}{a_t}\right)_{new}$$

provided that:

$$\beta_{old}\left(\frac{a_t}{a_s}\right)_{old} = \beta_{new}\left(\frac{a_t}{a_s}\right)_{new}$$

This condition can be satisfied if :

$$\left(\frac{a_s}{a_t}\right)_{new} = \left(\frac{a_s}{a_t}\right)_{old}\frac{1}{U_{0t}}$$

$$\beta_{new} = \beta_{old}\frac{1}{U_{0t}}$$

4.3 Measured Value of Anisotropy

As indicated in the previous section the value of a_t/a_s is rescaled by setting $U_{0t} = 1$. This is a natural choice since U_{Ct} is approximately unity in any case for small a_t. With this choice a_t/a_s undergoes little renormalization.

One must distinguish between the "bare" value of a_t/a_s which is input to this action and the physical or measured value of a_t/a_s . The reason is that the bare input value is renormalized by quantum effects.[13] [14] In an anisotropic lattice action there are two different couplings. One coupling multiplies terms sensitive only to the "spatial" length scale a_s. The other coupling multiplies terms sensitive to both a_s and a_t. These two couplings can (and do) run differently as these lattice spacings are sent to zero, and this shows up as a "renormalization" of the input anisotropy. More specifically, these two terms in the action get renormalized differently, and any such renormalization can be absorbed into a rescaling of a_t/a_s and β. When a_t/a_s is 1 then the "temporal" and "spatial" plaquettes are identical, so

there is no effect. The measured value of this ratio will become important later in calculating such things as lattice spacing and glueball mass. This measured value can be calculated by doing a simulation in which one of the "spatial" coordinates is used for Euclidean time instead of the "temporal" coordinate in the calculation of the Wilson loops.

On any lattice the Wilson loop calculation results in $W_{ST} = e^{-V(R)T}$ in the limit as $T \rightarrow \infty$. Here the subscript ST refers to a calculation where the T coordinate is the "temporal" coordinate direction. The value of T in this case is some integer times the a_t lattice spacing, $T = na_t$, and the Wilson loop is $W_{ST} = e^{-V(R)na_t}$. Therefore on an anisotropic lattice:

$$\tilde{V}_{ST}(R,T) = -\ln\left(\frac{W_{ST}(R,na_t)}{W_{ST}(R,(n-1)a_t)}\right) = a_t V(R,T)$$

and in the limit $T\rightarrow\infty$ this ratio becomes $\tilde{V}_{ST}(R) = a_t V(R)$.

Now if I do a Wilson loop where one of the "spatial" coordinates serves as a Euclidean time dimension, then $T = na_s$ and the Wilson loop is $W_{SS} = e^{-V(R)na_s}$, using the notation SS to denote two "spatial" dimensions. As a result:

$$\tilde{V}_{SS}(R,T) = -\ln\left(\frac{W_{SS}(R,na_s)}{W_{SS}(R,(n-1)a_s)}\right) = a_s V(R,T)$$

and in the limit $T\rightarrow\infty$ this ratio becomes $\tilde{V}_{SS}(R) = a_s V(R)$.

To get a determination of a_t/a_s, first an ultraviolet cutoff effect must be removed. $V(R) = \sigma R - \frac{b}{R} + V_0$ and this last term V_0 contains the self energies of the heavy quarks which is regulated by an ultraviolet cutoff which is not the same for SS and ST. The solution to this is to do a ΔV:

$$\frac{\tilde{V}_{ST}(R_2) - \tilde{V}_{ST}(R_1)}{\tilde{V}_{SS}(R_2) - \tilde{V}_{SS}(R_1)} = \frac{a_t}{a_s}$$

4.4 Scaling Lattice Spacing

The slope of the potential graph first seen in section 2.3.4 is modified to:

$$m = \frac{a_t\, V(R=n) - a_t\, V(R=m)}{\left(\frac{R}{a_s} = n\right) - \left(\frac{R}{a_s} = m\right)} = a_s\, a_t\, \frac{\Delta V}{\Delta R}$$

Thus the measured lattice spacing is:

$$a_s = \frac{\sqrt{m}}{\sqrt{\sigma}} \sqrt{\left(\frac{a_s}{a_t}\right)}$$

Chapter 5

Glueball Mass

Hadrons are made up of more elementary particles called quarks. The gauge particles that provide the strong binding force between the quarks are called gluons. The gluons act like spin raising and lowering operators because they change the colour (or colour "isospin" in SU(2)) of the quarks. Therefore unlike photons, the gauge particles of electromagnetism, the gluons carry a colour charge and can interact directly with each other. Due to confinement a state with net colour can never be seen; however, colour-singlet combinations of gluons ought to have finite energy. These bound states of gluons are referred to as gluonium or more commonly as glueballs.

5.1 Correlation Function

Recall that the trace of the plaquette $U_{\mu\nu}$ contains $(F^{\mu\nu})^2$ and that $F^{a}_{\mu\nu} = \partial^{\mu}A^{a}_{\nu} - \partial^{\nu}A^{a}_{\mu} + g f^{abc} A^{b}_{\mu} A^{c}_{\nu}$. The last term of this operator says that there are interactions between the gluons and this term can make the bound gluon states which are called glueballs. In general, $(F^{\mu\nu})^2$ can be interpreted as an operator which can create and destroy gluons. Then applying this operator to the vacuum state at two different times,

$\langle 0|Op(t)Op(0)|0\rangle$, will create some state made up of gluons at t=0 and annihilate the gluon state at t=t. In terms of plaquettes this expectation value is a Feynman path integral

$$\langle 0|Op(t)Op(0)|0\rangle = \prod_{\mu}\prod_{x}\int \left[dU_{\mu}(x)\right] e^{-S}\, U_{\alpha\beta}(t)\, U_{\gamma\delta}(0)$$

From quantum mechanics in Euclidean time the operator $Op(t) = e^{Ht}\, Op(0)\, e^{-Ht}$ where H is the Hamiltonian of the system. From this the glueball spectrum can be extracted:

$$C(t) = \sum_{n}|\langle n|O\rangle|^2 e^{-E_n t}$$

where $|O\rangle$ is the state created by applying Op(0) to the vacuum state. Similar to the Wilson loops, as t becomes large in euclidean time this correlation function will be dominated by the lowest energy state. Unfortunately this lowest state will be the vacuum state for an operator that transforms as a scalar under the rotation group. The glueball is the next higher state. Since the operator is made up of plaquettes, to remove the vacuum state from the sum subtract away the average plaquette $\langle \mathrm{Tr}\, U_{\mu\nu}\rangle = U_0^4$ from each plaquette. This will remove the vacuum state and give the next higher energy state. Then to extract the glueball mass define

$$m_g(t) \equiv -\ln\left(\frac{\langle 0|Op(t)Op(0)|0\rangle}{\langle 0|Op(t-1)Op(0)|0\rangle}\right)$$

and the actual ground state mass is given by the limit

$$m_g = \lim_{t\to\infty} m_g(t)$$

Since the lattice has periodic boundary conditions the maximum value of t has to be limited to t=T/2. After that value the correlation functions start wrapping back on

themselves. Therefore in order to get enough values to achieve a plateau the coordinate T should be reasonably large. This is another good reason to use an anisotropic lattice since the T coordinate will have more entries if the shape of the lattice is kept as a hypercube.

There is no preferred value T that corresponds to t=0. Therefore I use all values of T as the t=0 position and compute correlators for some separation ΔT. Then

$$m_g(\Delta T) \equiv -\ln\left(\frac{\sum_T \langle 0|Op(T+\Delta T)Op(T)|0\rangle}{\sum_T \langle 0|Op(T+\Delta T-1)Op(T)|T\rangle}\right)$$

and

$$m_g = \lim_{\Delta t\to\infty} m_g(\Delta t)$$

5.2 Scalar Glueball

The lowest glueball state is called the scalar glueball and has J=0. The trace of a plaquette will be used as the "Op" in the analysis of the previous section. A plaquette can be characterized by the normal to its surface. Now U_{12} can be represented schematically as an even function of the normal, since $U_{12} = U_{21}$ when traced. Under transformations of the cubic symmetry group U_{12} transforms like some function $a_1\hat{z}^2 + a_2\hat{z}^4 + \cdots$. Similarly, U_{13} is an even function of $\hat{y}$, etc.

Summing all "spatial" orientations $U_{12} + U_{13} + U_{23}$ gives a state that transforms like $(\hat{z}^2 + \hat{y}^2 + \hat{x}^2)$ and higher orders in $\hat{z}$, $\hat{y}$, $\hat{x}$. These higher order terms will correspond to states with higher J in the continuum limit. But these are expected to have higher energies and should decay faster as $T \to \infty$ than the lowest state excited by this operator which should

be the scalar glueball. Integrating over all "spatial" positions will give a rotationally and translationally symmetric object. For a fixed time slice in the continuum limit this is the rotationally symmetric glueball state with zero three-momentum, namely the scalar glueball. Using the standard notation of i and j for "spatial" coordinates, the operator then becomes

$$Op^{0^{++}} = Tr \sum_{\vec{x}} \sum_{\substack{i<j \\ j\neq i}} \left(U_{ij}(\vec{x},t) - U_0^4 \right)$$

5.3 Tensor Glueball

The lowest antisymmetric glueball state is called the tensor glueball and has J=2. Again think of the normal to the plaquette. Taking the difference of "spatial" orientations U_{12} - U_{13} gives a state that transforms like ($\hat{z}^2 - \hat{y}^2$) and higher orders in $\hat{z}$, $\hat{y}$. Integrating over all "spatial" positions will give an antisymmetric object, namely the tensor glueball state. The operator then becomes

$$Op^{2^{++}} = Tr \sum_{\vec{x}} \left(U_{12}(\vec{x},t) - U_{13}(\vec{x},t) \right)$$

which should have some overlap with the $J^P = 2^+$ state. In this case there is no need to subtract away the vacuum expectation value as it will cancel in any case, that is $J^P = 2^+$ has no overlap with the "scalar" vacuum.

In order to get the most statistics from a given configuration this operator was calculated using three combinations of orientations. Then the results were averaged. The "spatial" orientation combinations used were (12 - 13), (12 - 23) and (13 - 23).

Chapter 6

Fuzzing

In a conventional Wilson loop the spatial path between two lattice sites is chosen to be the shortest, namely a straight line. There are obviously many more paths connecting two sites. In fuzzing the straight line is smeared with other paths. [18] [19] Composite paths were first used to overcome the problem of the rapidly decreasing signal being lost in the noise in glueball mass calculations [18] [19] [32] and were later applied to potential calculations.[33]

The idea is to make operators that are closer to the size of the physical glueball or the quark-antiquark flux tube in the case of a potential calculation. The overlap of the glueball states with the simple plaquette operator gets smaller for smaller lattice spacings since the plaquette probes a smaller part of the physical state. Therefore by sampling many paths one can construct an extended or "fuzzy" operator which can probe more of the glueball wavefunction.

6.1 Fuzzing Method

Two parameters are used in fuzzing, the fuzzing constant (C) and the number of fuzzing iterations (N). Fuzzing is done on all the "spatial" links in the lattice using "spatial" staples. "Temporal" links are neither fuzzed nor used in the fuzzing process as this would destroy the

time evolution operator.

Fuzzy links are only used in calculating the observables. The original non-fuzzed links must still be used in the heat bath. Each configuration selected by the heat bath for measurement is made into a fuzzy configuration which is used to make the measurements. The heat bath continues to use the original configuration to develop subsequent configurations.

Fuzzing is done one link at a time over the entire lattice. The chosen link is multiplied by the fuzzing constant, then the four surrounding "spatial" staples are added in.

$$U_\mu^{\,n}(x) = CU_\mu^{\,n-1}(x) + \sum_{\substack{\pm\nu\neq\mu \\ \nu\neq 4}} U_{\pm\nu}^{\,n-1}(x)U_\mu^{\,n-1}(x\pm a\hat{\nu})U_{\pm\nu}^{\,n-1\dagger}(x+a\hat{\mu})$$

The resulting link is normalized by dividing by $|U_\mu^{\,n}(x)|$ to prevent overflow and to maintain simple SU(2) multiplicative tables. The result is saved in the fuzzy lattice replacing the old fuzzy link. The method I use is to determine the n^{th} iteration of all fuzzy links from the $(n-1)^{th}$ iteration. Then the n^{th} iteration of fuzzy links is saved in the fuzzy lattice replacing the $(n-1)^{th}$ iteration. The number of iterations determines how many times this process is repeated.

The larger the fuzzing constant the greater the contribution to the new fuzzy link from the original link and in the limit $C \to \infty$ fuzzing has no effect. The more iterations the greater the mixing of the surrounding staples.

6.2 Results of Fuzzing

The notation I use is (nn xx.x) where nn is the number of fuzzing iterations and xx.x is the fuzzing constant. Although nn=00 is sufficient to prevent fuzzing, the case of no fuzzing is given as (00 00.0) to avoid any confusion on my part.

The simulation runs consist of a 1,000 configuration thermalization from a cold start followed by a 100 configuration sampling selected from each tenth configuration of the next 1,000. The thermalization of 1,000 configurations is a bit of a trade off of accuracy versus time. While not sufficient to thoroughly thermalize the lattice it is completed in half a day of dedicated computer time whereas a 10,000 configuration thermalization would take 4 to 5 days. The 100 configuration sampling also takes half a day, so the duration is approximately 1 day on a dedicated computer for each trial for each of the seven β values. Using 4 time-shared computers at roughly 6 trials per β the whole thing took about 4 weeks.

I was searching here only for a reasonable estimate of the optimal fuzzing parameters. The runs used here were discarded, and were not used in the final quoted measurements.

As can be seen in Tables 6.1 and 6.2 and in Figure 6.1 the results are quite dramatic. The example I give in Table 6.1 is the static quark potential for R=1 of the 0.366 fm tadpole-improved case where β=0.848. Without fuzzing I cannot quite get a plateau, as described later in section 7.3, within 8 spacings. Whereas with fuzzing, a plateau is easily extracted after 4 or 5 spacings. As shown in table 6.2 with only 100 configurations the large errors make it very difficult to determine which fuzzing is best for optimizing the glueball mass. I used the same fuzzing parameters as for the static quark potential taking the T=1 mass as a fairly good indicator.

R=1				
T	**00 00.0**	**15 25.0**	**10 20.0**	**10 25.0**
1	0.9609(04)	0.8420(12)	0.8204(10)	0.8036(09)
2	0.8678(08)	0.7980(11)	0.7900(11)	0.7831(09)
3	0.8223(10)	0.7856(13)	0.7817(13)	0.7776(12)
4	0.8023(13)	0.7816(14)	0.7798(14)	0.7772(16)
5	0.7895(16)	0.7769(17)	0.7761(17)	0.7764(19)
6	0.7824(22)	0.7773(23)	0.7768(22)	0.7742(22)
7	0.7792(29)	0.7770(28)	0.7766(28)	0.7719(26)
8	0.7754(34)	0.7751(35)	0.7747(34)	0.7709(32)

Table 6.1 Effect of various fuzzing parameters on static quark potential.

Scalar Mass				
T	**00 00.0**	**15 25.0**	**10 20.0**	**10 25.0**
1	1.15(6)	0.99(5)	0.91(4)	0.86(4)
2	0.85(12)	0.79(10)	0.74(9)	0.76(8)
3	1.08(36)	0.54(15)	0.51(12)	0.85(18)
Tensor Mass				
1	1.53(6)	1.52(6)	1.46(5)	1.41(5)
2	1.21(16)	1.14(16)	1.19(15)	1.71(28)
3	0.87(42)	NA	NA	NA

Table 6.2 Effect of various fuzzing parameters on glueball mass.

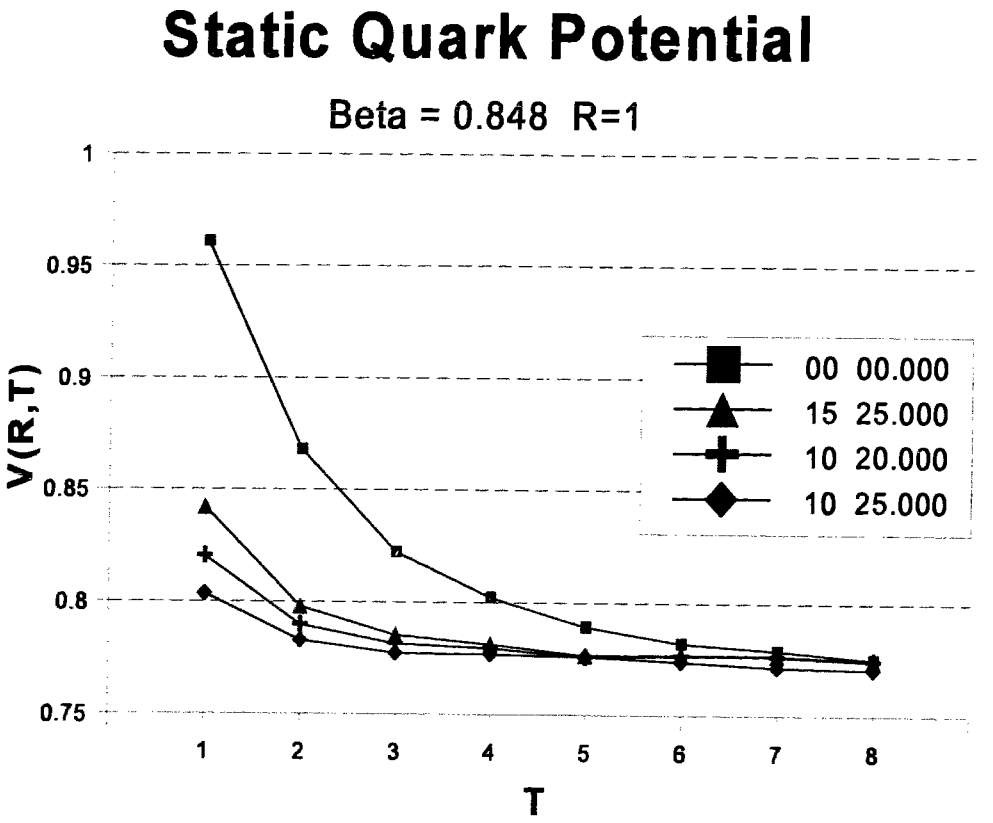

Figure 6.1 Impact of various fuzzing parameters on static quark potential.

β value	Number of Iterations	Fuzzing Constant
0.848	10	25.000
1.114	10	15.000
1.214	5	8.000
2.000	10	31.000
2.243	10	15.000
2.300	5	9.000
2.400	5	2.500

Table 6.3 Fuzzing parameters chosen for each β value.

As can be seen in table 6.3 the larger the lattice spacing the larger the fuzzing constant and vice versa. This is consistent with the idea stated earlier that large operators are needed to probe the glueball mass. The lattices with larger lattice spacing will require less fuzzing since their plaquettes are fairly large in the first place. Recall that the larger the fuzzing constant, the less smearing of nearby paths occurs.

Chapter 7

Results of Simulations

Simulations were run in order to make a comparison between the Wilson action and the tadpole-improved action. Simulations were run on lattices with spacing ranging from 0.1 fm to 0.4 fm. The entire assortment of simulations is summarized in table 7.1. In order to distinguish between the two sets of simulations, β_W will denote the coupling for Wilson action simulations and β_I will denote the coupling for tadpole-improved action simulations.

All simulations were run on shared computer resources at Simon Fraser University using code written in Fortran. In order to get more statistics some of the β values were run on several computers simultaneously and then the results combined in post processing.

Each simulation was started from a cold start. The heat bath was used to generate configurations. The first 10,000 of these configurations were skipped for thermalization. After that, configurations were selected for measurements after skipping enough configurations to minimize autocorrelations. A standard technique (for example see reference [34]) was used to determine the validity of these skipping values. For the lattices with larger spacing (greater than 0.2 fm) each tenth configuration was selected. For smaller spacing (less than 0.2 fm) each twentieth configuration was selected. The total number of configurations selected for measurements in each simulation varies based on the number of configurations required to reduce the errors sufficiently to give reasonable results.

β value	Lattice Spacing (fm)	Action	Lattice Size ($space^3$ x time)
β_I=0.848	0.366(1)	Tadpole-improved	8^3 x 32
1.114	0.238(1)	Tadpole-improved	8^3 x 20
1.214	0.202(2)	Tadpole-improved	10^3 x 20
β_W=2.000	0.355(2)	Standard Wilson	8^3 x 32
2.243	0.232(2)	Standard Wilson	8^3 x 20
2.300	0.203(1)	Standard Wilson	10^3 x 20
2.400	0.128(2)	Standard Wilson	12^3 x 12

Table 7.1 Summary of simulations.

7.1 Average Plaquette

The simplest measurement that can be taken from a lattice is the average plaquette. This value is defined as the average trace of each plaquette in all configurations used for measurements. This measure is useful in computer code debugging. The calculated values can frequently be compared to simulation results of other researchers as a first level check of computer code validity.

A summary of the average plaquette for each β value is given in table 7.2. The results are given for both the basic configurations directly from the heat bath and the configurations after fuzzing.

β value	Average Plaquette	Number of Configurations	Fuzzy Plaquette	Fuzzing Configurations
β_I=0.848	0.39594(6)	2,000	0.87053(1)	40,000
1.114	0.50330(7)	2,000	0.95638(1)	40,000
1.214	0.54639(5)	2,000	0.95466(2)	11,001
β_W=2.000	0.33313(9)	2,000	0.81737(2)	20,000
2.243	0.44327(9)	2,000	0.95089(1)	40,000
2.300	0.48309(6)	2,000	0.94086(2)	14,000
2.400	0.62999(4)	2,000	0.98970(1)	20,000

Table 7.2 Average plaquette before and after fuzzing for each β value.

7.1.1 U_0 used in Tadpole-Improved Heat Bath

The average trace of a lattice link U_0 is defined as the fourth root of the average plaquette since a direct trace of all the links would result in zero. U_0 is used in the tadpole-improved action. It is also used to remove the vacuum energy in the scalar glueball mass calculation.

The tadpole-improved action has a non-linearity since U_0, which appears in the action, must be determined from the average plaquette which itself is determined by the action. The value of U_0 used in the tadpole-improved heat bath is developed by an iterative procedure during the thermalization and then verified for consistency with the final value of U_0 determined from the entire simulation at the end of the run. Once set, the value of U_0 used in the tadpole-improved heat bath is not changed during the simulation.

To get the value of U_0 from the thermalization, I divide the 10,000 configurations used in the thermalization into twenty stages of 500 configurations each. For the first stage I use $U_0 = 1$ as a rough approximation. At the end of this first stage, I replace U_0 using the average plaquette from all configurations developed in the first stage. I repeat this process for the second stage. For the subsequent eighteen stages I keep a running average of U_0 and replace it at the end of each stage. At the end of the thermalization, the final running average of U_0 is saved and used for the entire simulation. Table 7.3 gives the values of U_0 at thermalization and at the end of simulation for the tadpole-improved simulations.

β_I value	Number of Configurations	Thermalized U_{0t}	Final U_{0f}	% Difference
0.848	40,000	0.96570(3)	0.96593(3)	0.023%
	32,000	0.96568(3)	0.96595(2)	0.027%
1.114	50,000	0.98865(3)	0.98891(2)	0.026%
	30,000	0.98868(3)	0.98890(3)	0.023%
1.214	11,001	0.98818(2)	0.98847(3)	0.029%
	5,300	0.98816(2)	0.98847(5)	0.031%

Table 7.3 Comparison of average link from thermalization and end of run.

7.2 Anisotropy

A major feature of this thesis is the use of anisotropic lattices. The "spatial" lattice spacing a_s is chosen in the range of about 0.1 fm to 0.4 fm. The "temporal" lattice spacing is kept around 0.1 fm and the anisotropy is introduced in the action by way of a_t/a_s. In the discussion any reference to lattice spacing means "spatial" lattice spacing, unless "temporal" is specifically stated.

7.2.1 Determining the β Value

One of the first tasks to be done before running a lattice simulation is to determine the β value which will give the desired lattice spacing. Fortunately for me the β values for several of the lattice spacings I was interested in had been determined by my supervisor in advance for other work he was doing. I had to determine the β values for the 10^3x20 anisotropic lattices that would give a lattice spacing of about 0.2 fm for both Wilson and tadpole-improved actions. I also had to determine the β value for the 8^3x20 anisotropic standard Wilson action lattice that would give a lattice spacing reasonably close to that for the 8^3x20 anisotropic tadpole improved action β_I=1.114. The results of this latter calculation are shown in detail.

This was a case of trial and error although some educated guesses could be made from data that I already knew. The results of the most notable trials that led me to β_W=2.243 are summarized in Table 7.4.

β_W value	Input a_t/a_s	Measured a_t/a_s	a_s (fm)
2.200	0.400	0.321	0.265
2.243	0.400	0.338	0.232
2.270	0.400	0.348	0.227
2.300	0.400	0.337	0.213
2.400	0.400	0.357	0.181

Table 7.4 Various trials to find a β value for an anisotropic Wilson action.

7.2.2 Lattice Spacings

The slope calculated in section 4.4 has to be adjusted for a 1/R term since the formula for the static potential between two quarks is of the form $V(R) = \sigma R - \frac{b}{R} + c$. This b coefficient is determined by looking for the least chi-squared fit to the integer potentials.

The lattice spacing a_s, the "temporal" lattice spacing a_t and the 1/R coefficient are given for each simulation in table 7.5. The determinations of a_t and a_t/a_s are discussed in the next section.

β value	σa_s^2	1/R coefficient (b)	Lattice spacing a_s (fm)	Time spacing a_t (fm)
β_I=0.848	0.667(2)	0.187(1)	0.366(1)	0.101(1)
1.114	0.283(1)	0.255(2)	0.238(1)	0.097(2)
1.214	0.205(1)	0.252(2)	0.202(2)	0.101(2)
β_W=2.000	0.630(2)	0.101(1)	0.355(2)	0.071(3)
2.243	0.268(1)	0.217(1)	0.232(2)	0.078(2)
2.3	0.206(1)	0.211(1)	0.203(1)	0.087(2)
2.4	0.082(1)	0.214(2)	0.128(2)	0.128(2)

Table 7.5 Results of potential fits for each simulation.

7.2.3 Anisotropy Results

To illustrate the data obtained in the many simulations, the plateaux of the static quark potentials V(R) for both "spatial" Wilson loops (SS) and mixed "spatial"/"temporal" Wilson loops (ST) are as shown in Table 7.6 for the 0.2 fm tadpole-improved and Wilson actions. The results are graphed in figures 7.1 and 7.2. To make the plots comparable, the ST values are rescaled using the input a_t/a_s and then the SS values are shifted so that they agree with the ST results at $R = a_s$. The line is fitted to the ST values. The noticeably different slopes of the SS values shows the renormalization of a_t/a_s in the Wilson action.

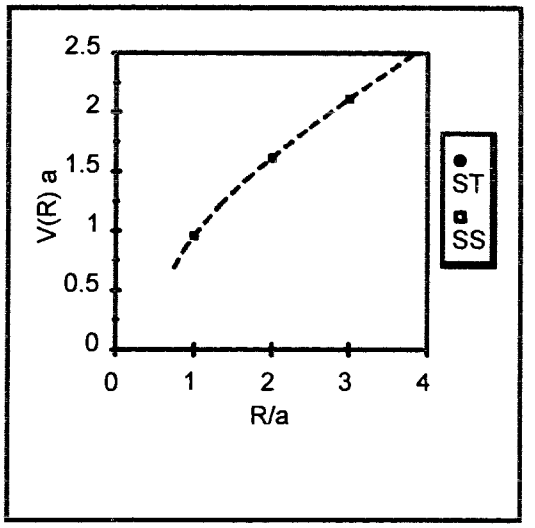

Figure 7.1 Static quark potential in different orientations for β_I=1.214.

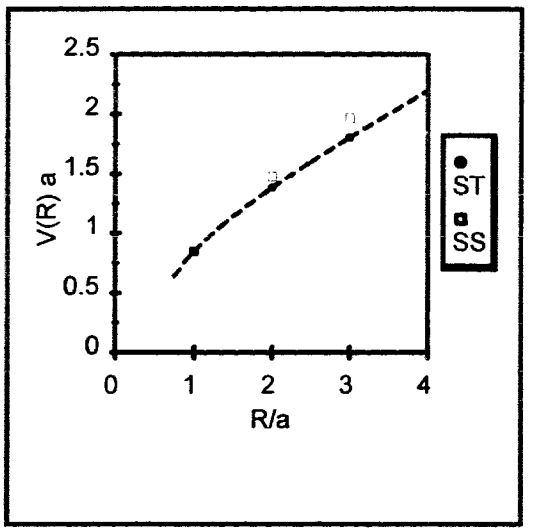

Figure 7.2 Static quark potential in different orientations for β_W=2.300.

β value	Loop	V(R=1)	V(R=2)	V(R=3)
β_I=1.214	ST	0.4788(4)	0.8085(14)	1.0572(33)
	SS	1.112(1)	1.767(3)	2.266(16)
β_W=2.300	ST	0.4241(3)	0.6921(13)	0.9031(32)
	SS	1.159(1)	1.787(9)	2.279(12)

Table 7.6 Static quark potential for SS and ST Wilson loops.

The ratio of a_t over a_s was calculated from the results in table 7.6 as discussed in chapter 4 and these results are shown in table 7.7 including the results from all other anisotropic simulations done. A comparison between input a_t/a_s and measured a_t/a_s is made in Table 7.8 for these actions.

β value	R2-R1	R3-R1	R3-R2	Average
β_I=0.848	0.277(2)	0.276(3)	0.282(6)	0.278(2)
1.114	0.416(5)	0.415(6)	0.415(16)	0.415(6)
1.214	0.503(4)	0.501(8)	0.498(13)	0.501(7)
β_W=2.000	0.199(4)	0.204(10)	0.196(22)	0.200(8)
2.243	0.335(23)	0.338(45)	0.341(104)	0.338(38)
2.300	0.427(5)	0.428(8)	0.429(18)	0.428(7)

Table 7.7 Ratio of a_t over a_s for anisotropic lattices.

β value	a_t/a_s input	a_t/a_s measured	Difference	% Difference
β_I=0.848	0.276	0.278(2)	-0.002	-0.7%
1.114	0.409	0.415(6)	-0.006	-1.4%
1.214	0.500	0.501(7)	-0.001	-0.2%
β_W=2.000	0.250	0.200(8)	0.050	20.0%
2.243	0.400	0.338(8)	0.062	18.3%
2.300	0.500	0.428(7)	0.072	16.8%

Table 7.8 Comparison of input a_t/a_s to measured for anisotropic lattices.

As can be seen in table 7.8 the renormalizations from quantum effects are much larger in the Wilson actions than for the tadpole-improved actions. This result is generally true. Unimproved lattice actions can show very large renormalizations [4], but most of these renormalizations come from tadpoles which have been divided out of the improved action, leaving only small renormalizations. For the tadpole-improved actions the difference between input and measured values is within errors, so no later scaling adjustments were done.

7.3 Static Heavy Quark Potential

The static heavy quark potential was calculated for all seven β values. In all cases 2,000 configurations were used to determine the potential. This number of configurations in the ensemble was sufficient to reduce the errors enough to get meaningful results.

For brevity I have shown the detailed results of V(R,T) for only one of the simulations along with a small sampling of other results in graphical form. Table 7.9 shows the V(R,T) results for β_I=0.848 with the plateau values V(R) highlighted. Representative graphs of V(R,T) are shown in figures 7.3 and 7.4.

	R=1	R=2	R=3	R=4
T	V(R,T)	V(R,T)	V(R,T)	V(R,T)
1	0.8044(2)	1.6062(5)	2.3816(8)	3.1525(11)
2	0.7838(2)	1.5592(6)	2.2940(12)	3.0192(19)
3	0.7787(3)	1.5464(8)	2.2638(17)	2.9663(31)
4	0.7771(3)	1.5410(11)	2.2460(26)	2.9271(61)
5	**0.7767(4)**	1.5384(15)	2.2364(43)	**2.918(12)**
6	0.7769(5)	**1.5371(21)**	**2.2340(75)**	2.923(26)
7	0.7771(6)	1.5393(30)	2.225(13)	2.854(53)
8	0.7767(7)	1.5361(45)	2.200(23)	2.58(10)
	R=Sqrt2	R=Sqrt3	R=Sqrt5	R=Sqrt8
1	1.2417(4)	2.3665(7)	1.8743(7)	2.3553(9)
2	1.1840(5)	1.4837(9)	1.7756(9)	2.2169(13)
3	1.1719(6)	1.4566(13)	1.7516(12)	2.1786(17)
4	1.1685(7)	1.4478(19)	1.7432(16)	2.1620(26)
5	**1.1679(9)**	**1.4447(25)**	1.7392(23)	2.1551(41)
6	1.1688(11)	1.4449(38)	**1.7393(34)**	**2.1561(69)**
7	1.1683(15)	1.4389(55)	1.7395(51)	2.144(11)
8	1.1651(20)	1.4454(82)	1.7366(78)	2.146(20)

Table 7.9 Tadpole-improved action V(R,T) for β value 0.848.

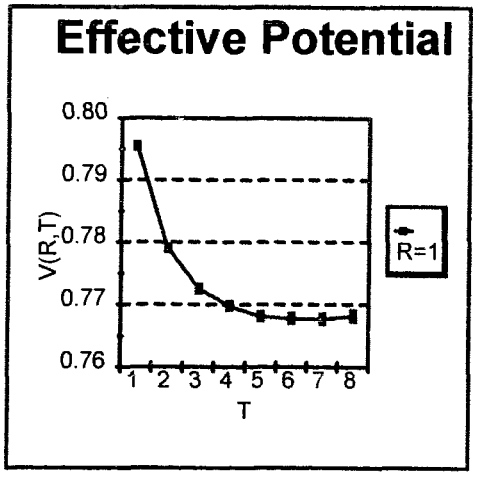

Figure 7.3 Wilson action V(R=1,T) for β_W=2.000.

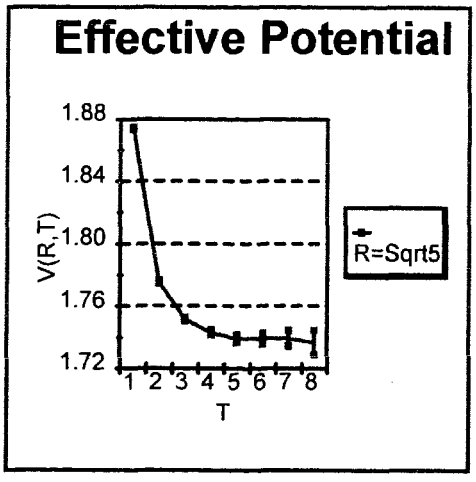

Figure 7.4 Tadpole-improved action V(R=$\sqrt{5}$,T) for β_I=0.848.

The plateau value V(R) for a specific R value is determined from the various V(R,T) entries based on their value and error. Subjectively the graph has to look similar to figures 7.3 and 7.4 in order to determine the plateau value. All the V(R,T) graphs from all simulations looked like these representative figures. I look for two or three successive T values for which the data V(R,T) overlap within statistical errors. An estimate of systematic error in the extrapolated V(R) is then taken from the statistical error of the largest T value

in the plateau.

Examples of the static heavy quark potential V(R) results for representative β values are shown in figures 7.5 and 7.6. In all these figures the filled in circles represent the on-axis potentials while the open circles represent the off axis potentials. Table 7.5 gave the coefficients of the best fit line $V(R) = \sigma R - b/R + c$ which had been calculated using the least chi-squared fit to the integer potentials for each β value. These fitted lines have been superimposed on figures 7.5 through 7.6. As presented in section 4.4 the lattice spacings are calculated from the slope of the various curves. These spacings were summarized in table 7.1.

Figure 7.7 and table 7.10 show a comparison of the actual to fitted values for the off axis potentials. In the figure the lines are fitted to the Wilson action on-axis potentials and the percentages in table 7.10 are used to plot the off-axis points. Both figure and table show that for any given lattice spacing the off axis potential is much closer to that calculated from integer potentials for the tadpole-improved potential than for the Wilson potential. This also shows that generally the off axis potentials are much closer to those calculated from the integer potentials for the smaller spacing lattices than for the larger spacing lattices.

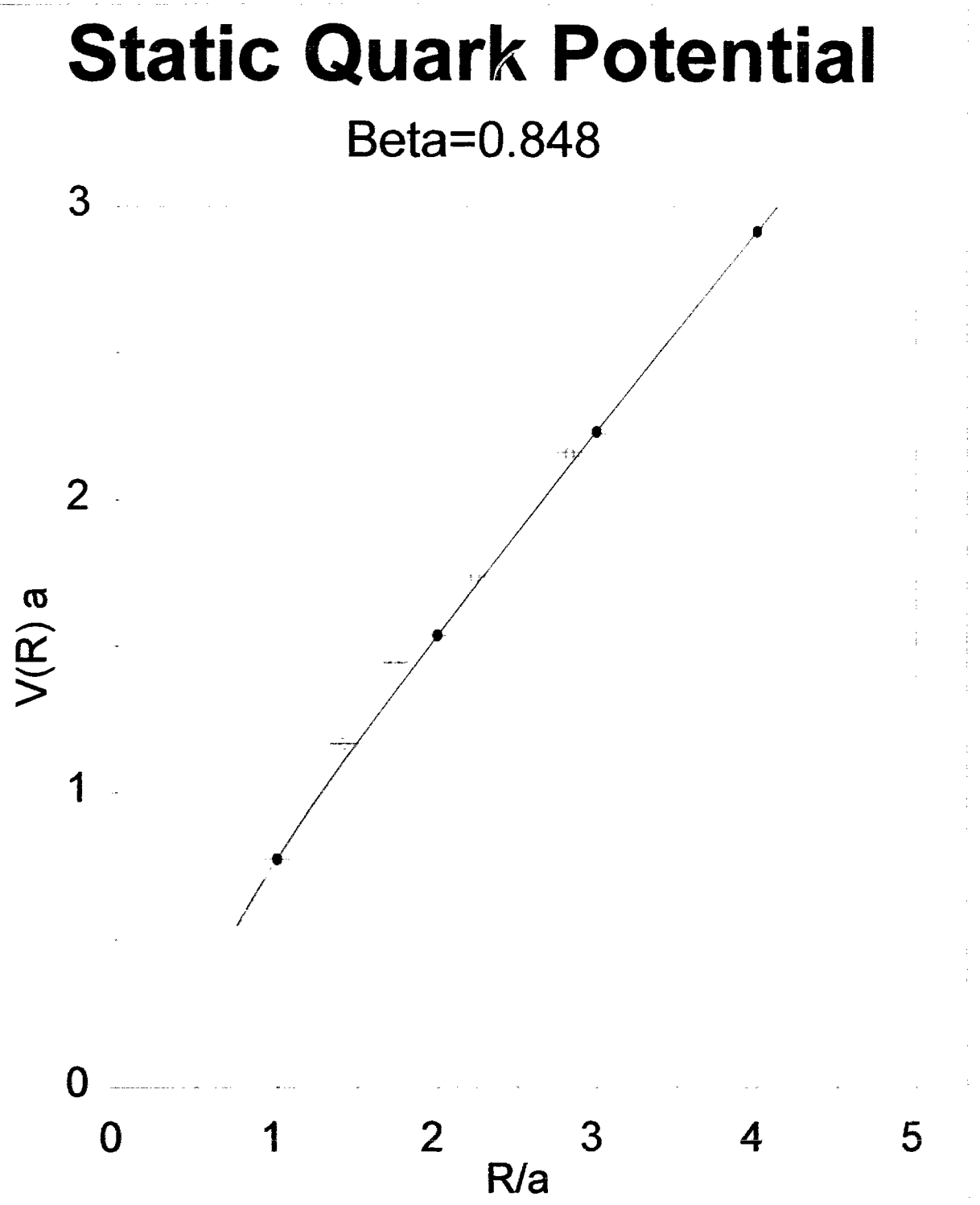

Figure 7.5 Static quark potential for 0.366 fm tadpole-improved action

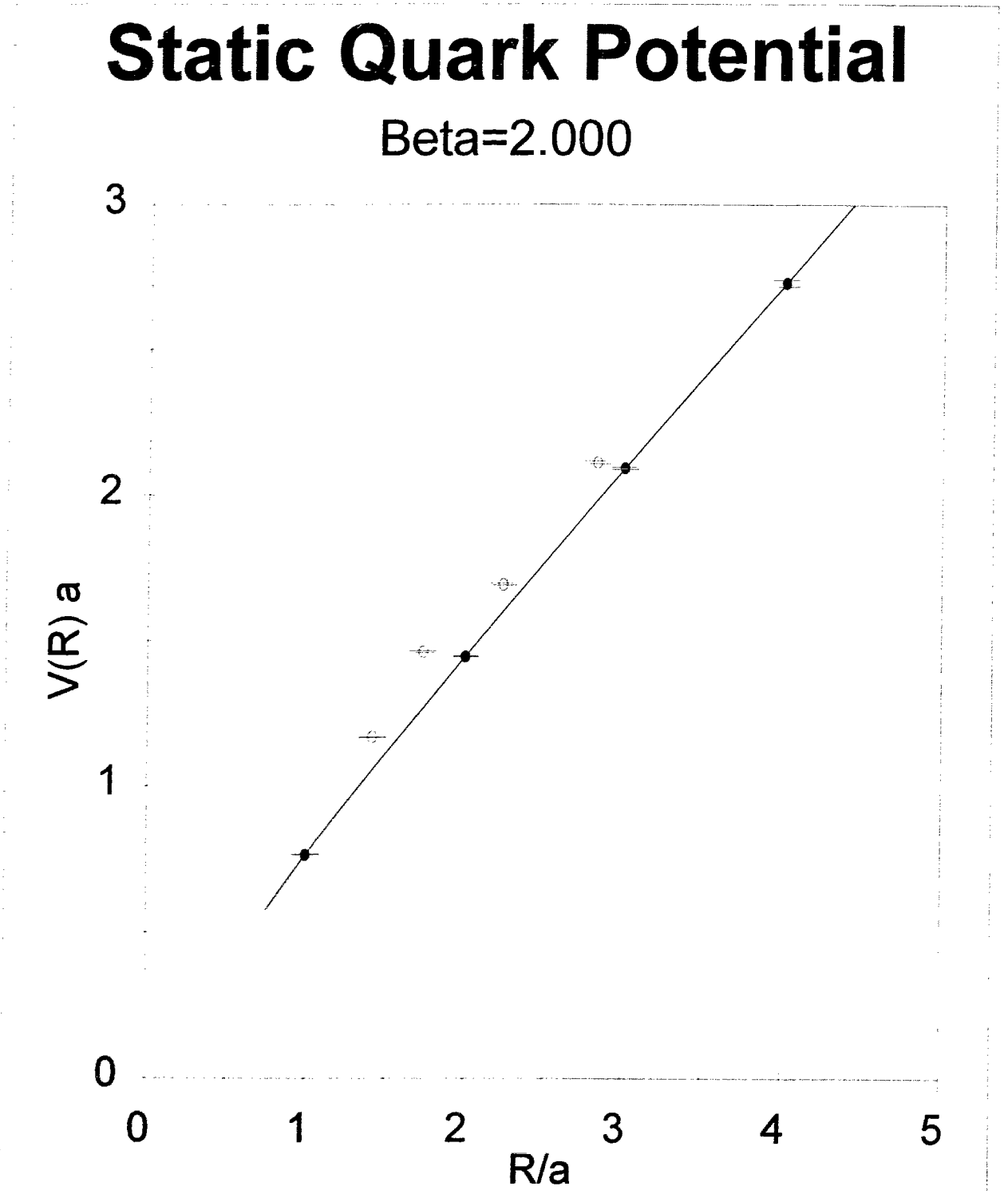

Figure 7.6 Static quark potential for 0.355 fm Wilson action

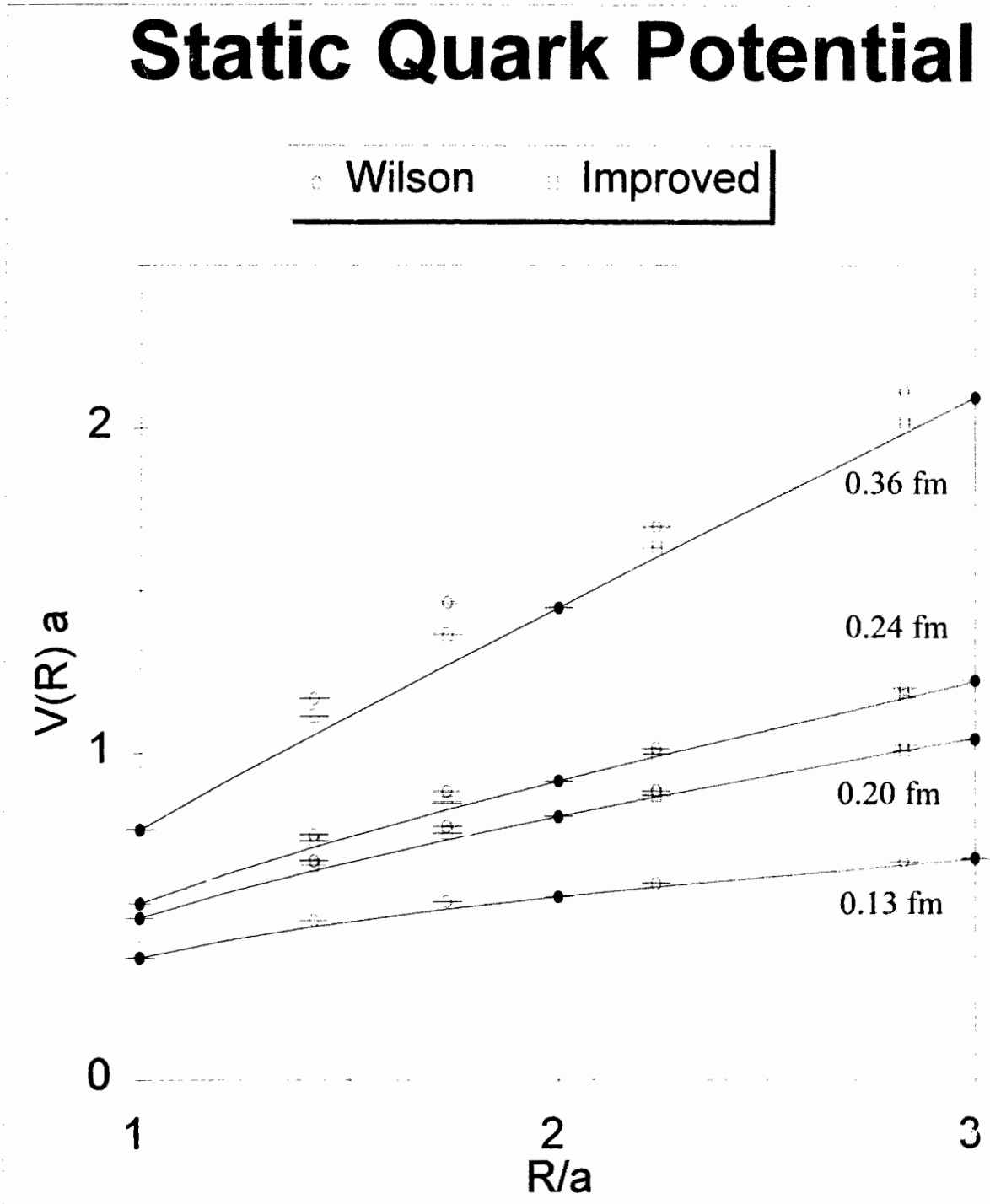

Figure 7.7 Comparison of off axis static quark potentials

β value	$\sqrt{2}$	$\sqrt{3}$	$\sqrt{5}$	$\sqrt{8}$
β_I=0.848	5.4%	7.5%	2.1%	1.9%
1.114	2.7%	2.6%	0.7%	0.4%
1.214	2.6%	2.9%	0.6%	-0.1%
β_W=2.000	10.6%	15.1%	5.9%	6.6%
2.243	5.2%	6.7%	2.5%	2.7%
2.300	4.8%	5.6%	2.0%	1.8%
2.400	4.1%	4.4%	1.8%	1.5%

Table 7.10 Deviation of off-axis potentials from fit to on-axis data.

The difference from calculated potentials is approximately the same for the 0.232 fm Wilson action (β_W=2.243) as for the 0.366 fm tadpole improved action (β_I=0.848). Typically the required computer time scales as a^{-6} which would mean that the smaller spacing would require 15 times as much computer resources as the larger spacing. In my simulations the code for tadpole-improvement adds approximately fifty percent to the resources used by the simulation. While I have no proof that this can be extrapolated to other lattice spacings, here I see an approximately tenfold improvement in doing static quark potential calculations using tadpole-improvement.

7.4 SU(2) Glueball Mass

The masses of both the Scalar and Tensor glueballs were calculated in simulations for each β value. The number of configurations for each β value varies depending on what was required to reduce the statistical error so that the results were meaningful. The number of configurations used for measurement for each β value is given in table 7.11.

β value	Number of Configurations
β_I=0.848	72,000
1.114	80,000
1.214	16,301
β_W=2.000	20,000
2.243	40,000
2.3	14,000
2.4	33,500

Table 7.11 Number of configurations for each β value.

An estimate of the large T extrapolation of the mass is required. The procedure used here is somewhat different from that used for the static quark potential where the errors were sufficiently small that a plateau estimate seemed reliable enough. In this case the data points $m_g(T)$ are fitted in a range of T values from T_{min} to T_{max} to a curve $C e^{-MT}$. T_{min} must be large enough to eliminate excited states within statistical errors. Holding T_{max} fixed a value of $M(T_{min})$ is determined from $C e^{-MT}$ for successive T_{min} values. M is chosen based on the statistical overlap between two successive $M(T_{min})$ values.

7.4.1 SU(2) Scalar Glueball

For brevity I have only shown the detailed results for the mass of the scalar glueball from one of the simulations. Table 7.12 shows the mass of the scalar glueball results for β_I=0.848 with the exponential fit $\frac{M}{\sqrt{\sigma}}$ highlighted.

T	$\frac{m_g(T)}{\sqrt{\sigma}}$	T_{min}	$\frac{M(T_{min})}{\sqrt{\sigma}}$
1	3.92(1)	1	3.54(2)
2	3.56(2)	2	**3.51(4)**
3	3.50(3)	3	3.52(9)
4	3.49(7)	4	3.58(17)
5	3.6(2)	5	3.54(35)
6	3.5(4)		
7	3.2(7)		
8	5.5(28)	T_{max}	

Table 7.12 Scalar glueball mass for β_I=0.848.

Figures 7.8 and 7.9 show representative graphs of $\frac{m_g(T)}{\sqrt{\sigma}}$ versus T for the scalar glueball mass at selected β values. In these graphs the solid line with the two dashed lines shows the exponential fit $\frac{M}{\sqrt{\sigma}}$, along with one sigma errors.

Figure 7.10 shows a comparison of the SU(2) scalar glueball masses based on lattice spacing. Also shown in the figure are data points taken from the literature [23] [32] and an extrapolated continuum value.[35]

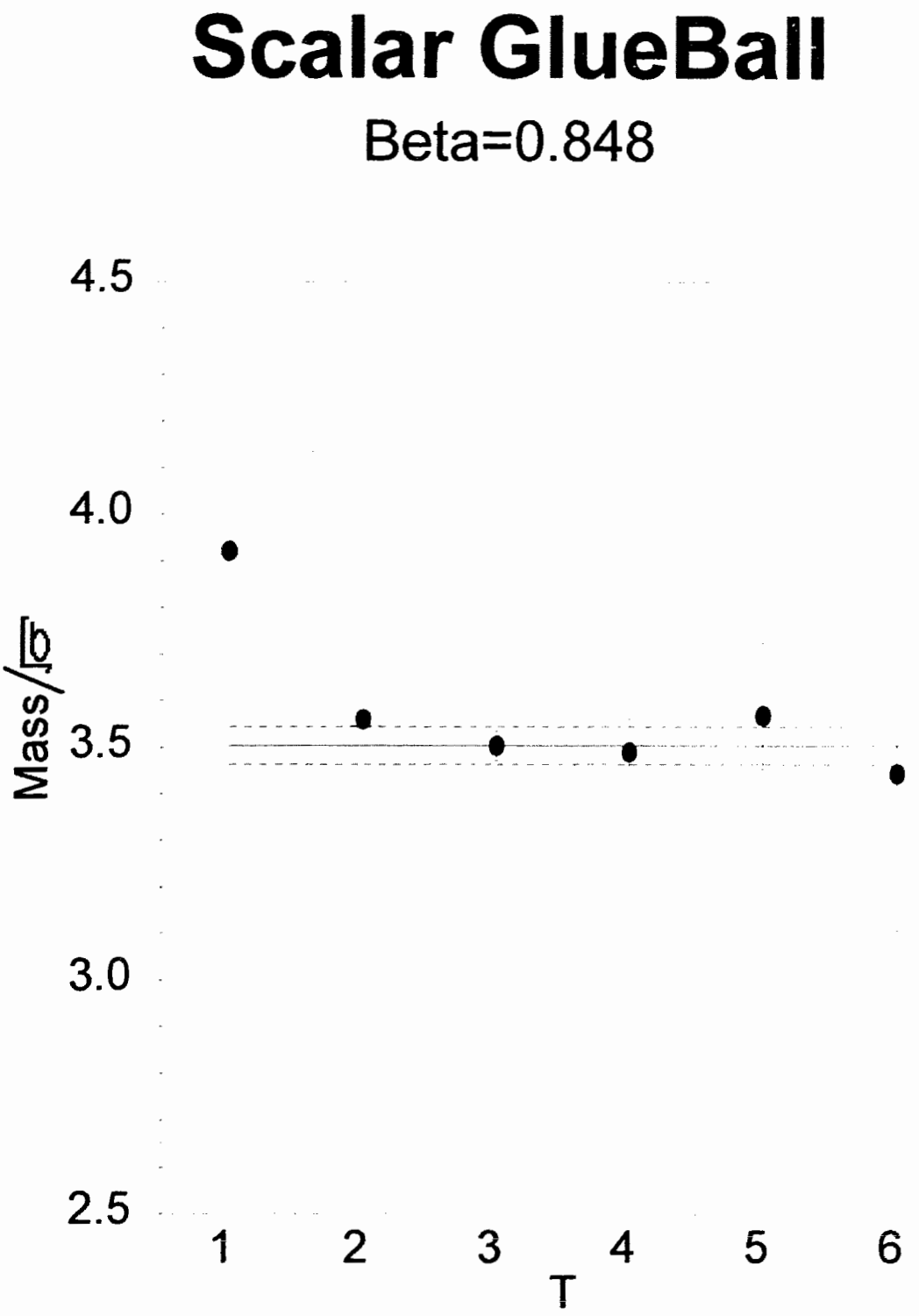

Figure 7.8 Scalar glueball mass for 0.366 fm tadpole-improved action

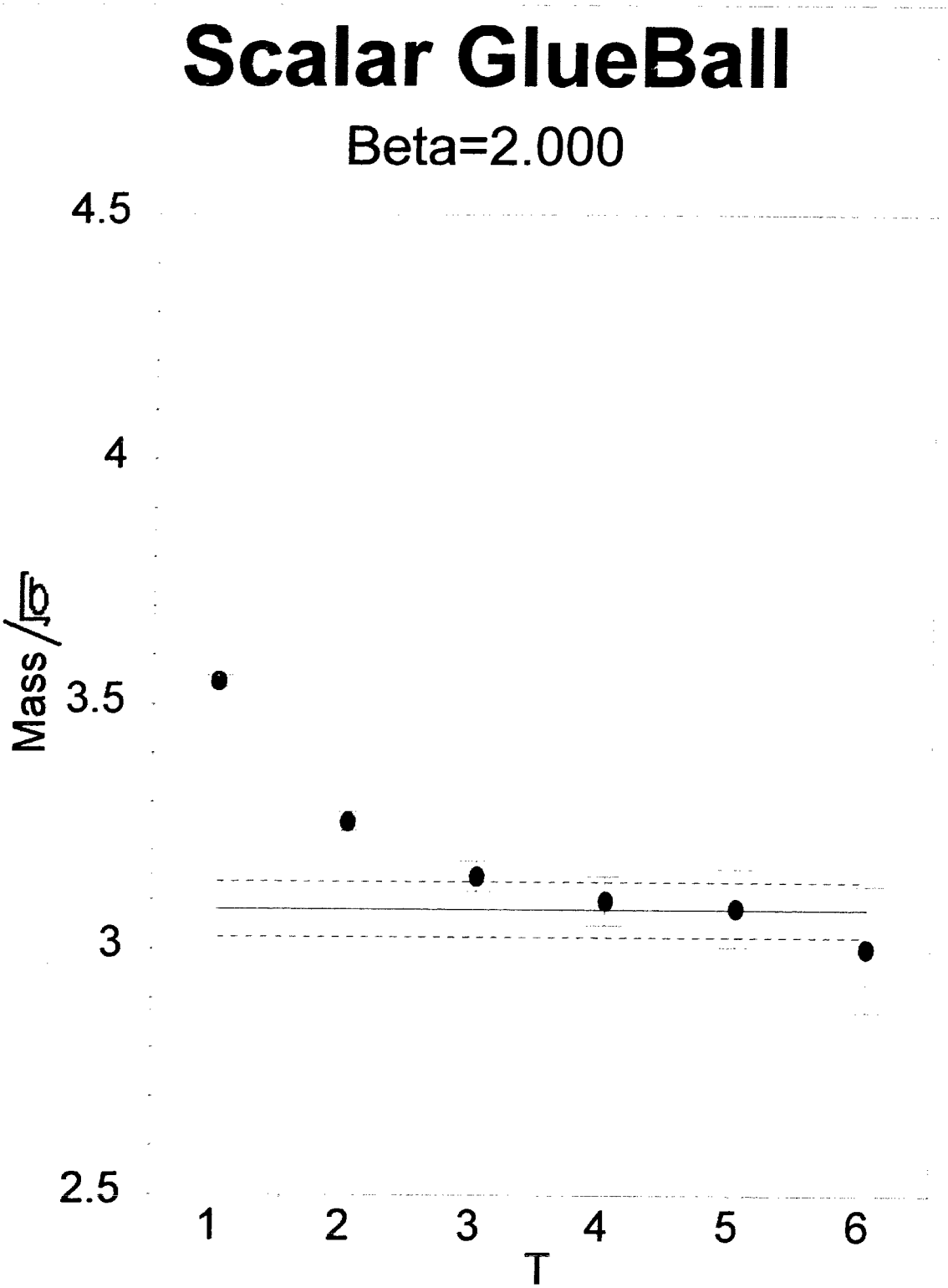

Figure 7.9 Scalar glueball mass for 0.355 fm Wilson action

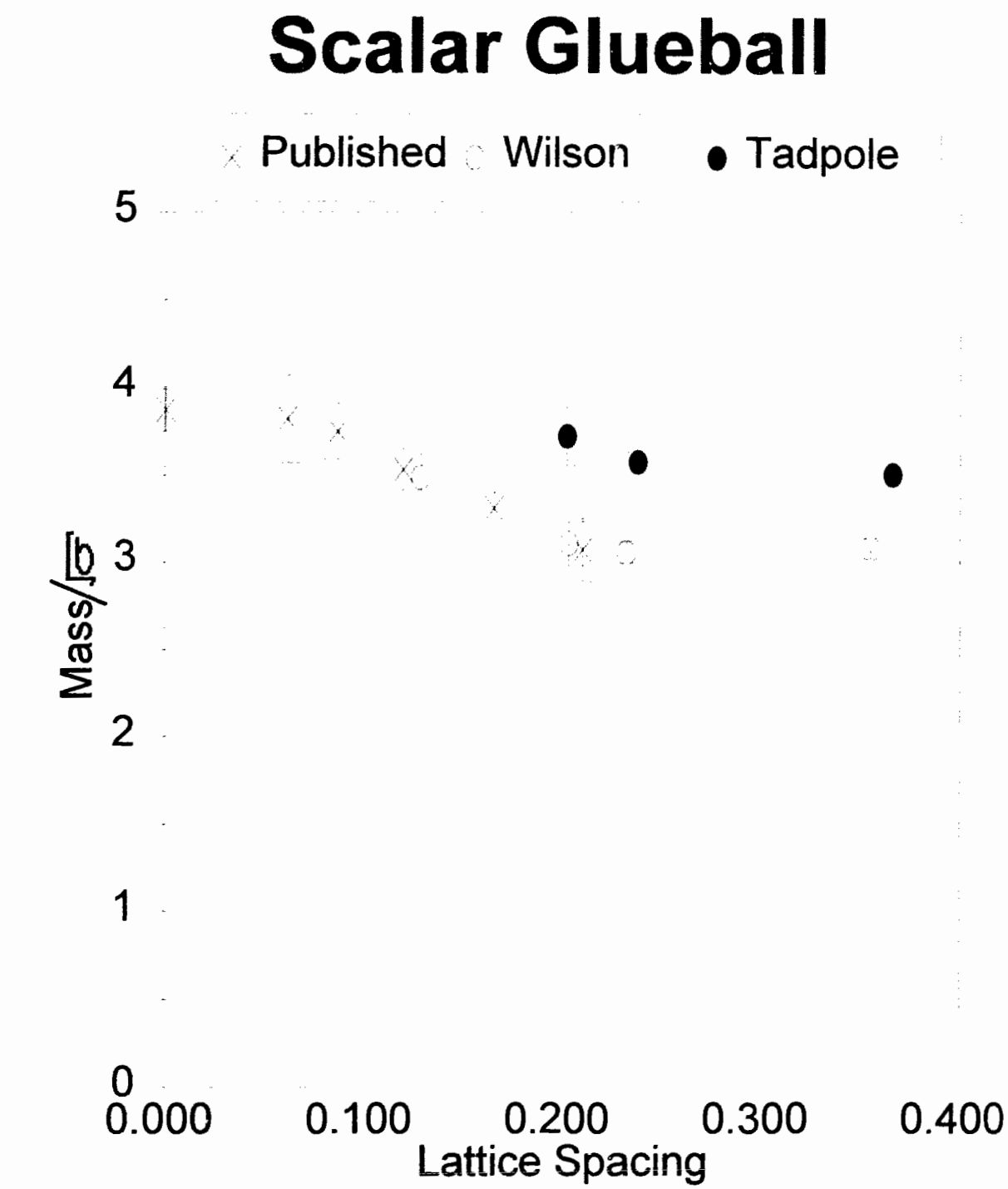

Figure 7.10 Comparison of Scalar glueball masses

Table 7.13 shows a comparison of the SU(2) scalar glueball mass values to the continuum value. The last column shows the number of standard errors that the central value of the scalar mass is away from the cental value of the continuum mass.

β value	Lattice Spacing (fm)	$\frac{M}{\sqrt{\sigma}}$	% Difference from Continuum	Number of σ from Continuum
Continuum		3.87(12)		
β_I=0.848	0.366(1)	3.51(4)	-9.4%	9
1.114	0.238(1)	3.57(5)	-7.7%	6
1.214	0.202(2)	3.72(17)	-3.9%	1
β_W=2.000	0.355(2)	3.08(6)	-20.4%	14
2.243	0.232(2)	3.06(6)	-21.0%	13
2.300	0.203(1)	3.11(13)	-19.8%	6
2.400	0.128(2)	3.49(13)	-9.9%	3

Table 7.13 Comparison of calculated scalar glueball mass to continuum value.

As can be seen in Figure 7.10 and Table 7.13 the tadpole-improved actions resulted in scalar glueball mass values which are significantly closer to the continuum value than the Wilson actions. The difference from continuum is approximately the same for the 0.128 fm Wilson action (β_W=2.400) as for the 0.366 fm tadpole improved action (β_I=0.848). As

previously stated, the required computer time typically scales as a^{-6} which would mean that the smaller spacing would require 550 times as much computer resources as the larger spacing. In my simulations the code for tadpole-improvement adds approximately fifty percent to the resources used by the simulation. While I have no proof that this can be extrapolated to other lattice spacings, here I would see a 350 fold improvement in doing scalar glueball mass calculations using tadpole-improvement if exactly the same physical volumes were used and if the skips between measurements were actually scaled by $1/a^2$.

The lattice spacing for the Wilson action must drop below 0.2 fm before any significant approach to the continuum value is seen. The tadpole improved action goes towards the limit even at 0.4 fm, although to drop below 5% error requires a lattice spacing of about 0.2 fm. This could suggest that the scalar glueball may be unusually small in SU(2).

7.4.2 SU(2) Tensor Glueball

For brevity I have only shown the detailed results of the mass of the tensor glueball for two of the simulations. Figures 7.11 and 7.12 show graphs of the tensor glueball mass for selected β values. In these graphs the solid line with the two dashed lines shows the exponential fitted $\frac{M}{\sqrt{\sigma}}$, including errors.

Figure 7.13 shows a comparison of the SU(2) tensor glueball masses based on lattice spacing. Also shown in the figure are data points taken from the literature [23] [32] and an extrapolated continuum value. [35]

Table 7.14 shows a comparison of the SU(2) tensor glueball mass values to the continuum value.

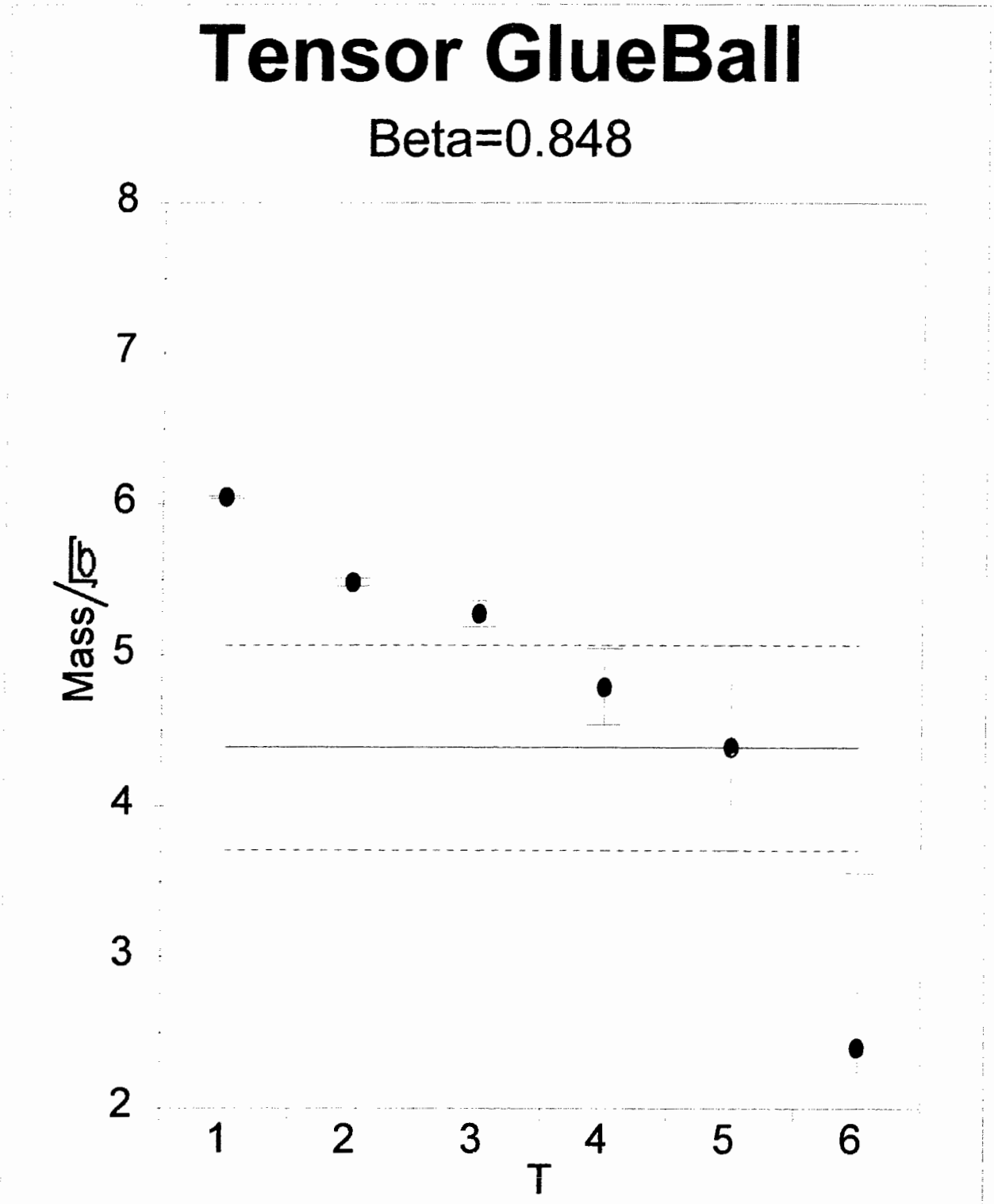

Figure 7.11 Tensor glueball mass for 0.366 fm tadpole-improved action

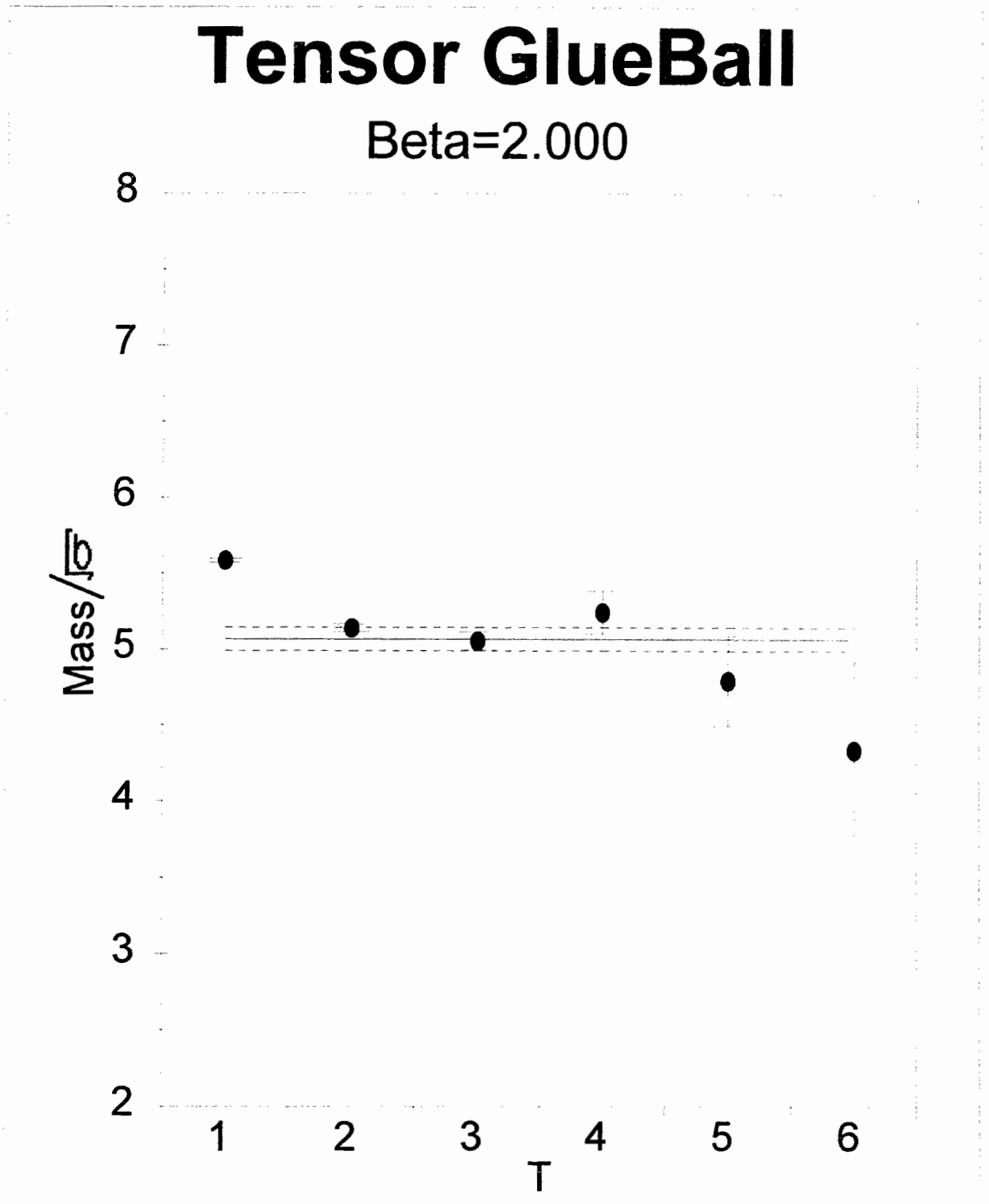

Figure 7.12 Tensor glueball mass for 0.355 fm Wilson action

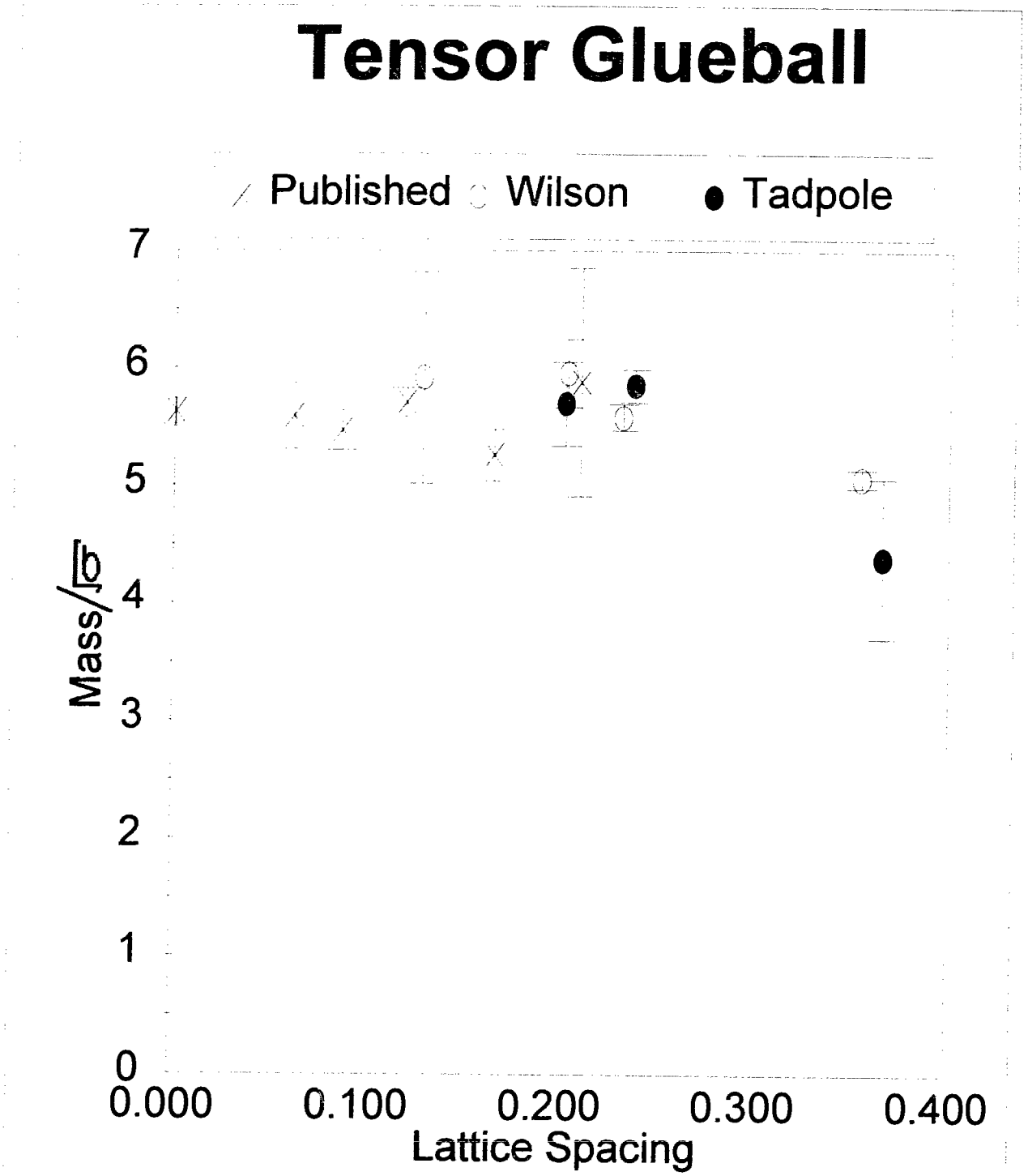

Figure 7.13 Comparison of tensor glueball masses

β value	Lattice Spacing (fm)	$\frac{M}{\sqrt{\sigma}}$	% Difference from Continuum	Number of σ from Continuum
Continuum		5.63(11)		
β_I=0.848	0.366(1)	4.39(68)	-22.1%	2
1.114	0.238(1)	5.85(14)	3.9%	2
1.214	0.202(2)	5.70(36)	1.2%	<1
β_W=2.000	0.355(2)	5.07(8)	-10.0%	7
2.243	0.232(2)	5.58(11)	-0.9%	<1
2.300	0.203(1)	5.95(29)	5.8%	1
2.400	0.128(2)	5.92(90)	5.1%	<1

Table 7.14 Comparison of calculated tensor glueball mass to continuum value.

As can be seen in Figure 7.13 and Table 7.14 the tadpole-improved actions resulted in tensor glueball mass values which are approximately the same as the Wilson actions. However the very large errors in the β_I=0.848 data prevents reaching any definite conclusions. More data is needed.

There is a large difference between the lattices with the largest spacing and all other lattices for both tadpole-improved and Wilson actions. Namely making the tadpole-improved lattice spacing 0.238 fm (β_I=1.114) gave a significant improvement in the results over 0.366 fm spacing (β_I=0.848). This would suggest that the tensor glueball is larger than the scalar glueball, as one might expect.

Chapter 8

Conclusions

The objective of this thesis has been a detailed comparison of lattice gauge theory simulations under SU(2) colour with and without tadpole-improvement. Calculations have been done for lattice anisotropy, static quark potential, mass of the scalar glueball and mass of the tensor glueball. The lattice spacings were in the range of 0.1 fm to 0.4 fm. In the case of the glueball masses the results were also compared with published results from simulations on small lattices in the less than 0.1 fm range.

A significant feature of this thesis has been the use of anisotropic lattices. The "spatial" lattice spacing a_s was in the range of 0.1 fm to 0.4 fm. The "temporal" lattice spacing was kept around 0.1 fm. The use of anisotropic lattices allowed easier determination of the scalar and tensor glueball masses since more measurements of the correlation functions could be established before they disappeared into the noise.

Another tool used to more easily extract the signals was fuzzing. This entailed the use of smeared paths to increase the overlap with the ground state. The effects on the calculation of the static heavy quark potential were demonstrably dramatic. In the calculation of the glueball masses the effects were similar to that of the potential. In the case of the β=1.114 (tadpole-improved action on the 0.238 fm spacing lattice) tensor glueball, no plateau could be found without using fuzzing.

The results of the comparisons of the tadpole improved actions to the standard Wilson actions showed significant gains for most observables measured.

The renormalizations from quantum effects are much larger in the Wilson actions than for the tadpole-improved actions. Unimproved lattice actions tend to show very large renormalizations, but most of these renormalizations come from tadpoles which have been divided out of the improved action, leaving only small renormalizations. For the tadpole-improved actions the difference between input anisotropy and measured anisotropy is within errors and therefore not statistically significant.

In the case of the static heavy quark potential, the breaking of rotational invariance is much smaller for the tadpole-improved action than for the Wilson action. Rotational symmetry breaking provides a direct measure of discretization errors in the lattice action. For any given lattice spacing the off axis potential is much closer to interpolations of the integer potentials for the tadpole-improved potential than for the Wilson potential. Also as expected, rotational symmetry breaking was reduced for lattices with smaller lattice spacing. The measured symmetry breaking is approximately the same for the 0.232 fm spacing Wilson action as for the 0.366 spacing tadpole-improved action. Since the required computer time scales as a^{-6} the smaller spacing would require approximately 15 times as much computer resources as the larger spacing. Tadpole-improvement routines add approximately fifty percent overhead to the computing resources required, because of the greater complexity of the action. Therefore this case resulted in an approximate tenfold decrease in computing resources required to do the static potential calculations using the tadpole-improved action.

The tadpole-improved actions resulted in scalar glueball mass values which were significantly closer to the continuum value than the Wilson actions. The difference from continuum is approximately the same for the 0.128 fm Wilson action as for the 0.366 fm tadpole improved action. Taking into account the required computer time scaling of a^{-6} and the fifty percent overhead of tadpole-improvement this data suggests a 350 fold improvement

in doing scalar glueball mass calculations using tadpole-improvement. This is a day versus a year to get the same results.

The lattice spacing for the Wilson action must drop below 0.2 fm before any significant approach to the continuum scalar glueball mass value is seen. In the case of the tadpole improved action, a significant drop in discretization errors also requires a lattice spacing below about 0.2 fm. This could suggest that the scalar glueball may be unusually small in SU(2). A similar conclusion was suggested for SU(3) glueballs by Morningstar and Peardon. [17]

Preliminary results for the tensor glueball mass were presented. The tadpole-improved actions resulted in tensor glueball mass values which are approximately the same as the Wilson actions, but very large statistical errors on the coarsest lattice prevented a definitive comparison. There is a large difference between the lattices with the largest spacing and all other lattices for both tadpole-improved and Wilson action. Namely making the lattice spacing 0.238 fm gave a significant improvement in the results over 0.366 fm spacing. This could suggest that the tensor glueball is somewhat larger than the scalar glueball, as one might expect. On the other hand, the large errors in the 0.366 fm tadpole-improved action results (β=0.848) require more work. A better optimization of the fuzzing tailored specifically for the tensor glueball may help here.

As suggested in section 3.2 a potential future research project could be to determine if there is a better definition of the average lattice link than using the fourth root of the average plaquette. A definition based on the average link with a specific gauge fixing has been made. [30] Another major project would be to do the same research under SU(3).

For the most part the research was successful. I have demonstrated that state-of-the-art calculations can be done on small computers using large lattice spacings with tadpole-improvement. The results are reasonably close to those obtained using smaller lattice spacings which in the past have required a much longer time frame using larger computers.

Bibliography

[1] K. G. Wilson. Confinement of Quarks. Physical Review D, 10:2445, 1974.

[2] C. T. H. Davies, G. G. Batrouni, G. R. Katz, A. S. Kronfeld, G. P. Lepage, P. Rossi, B. Svetitsky and K. G. Wilson. Fourier Acceleration in Lattice Gauge Theories. III. Updating Field Configurations. Physical Review D, 41:1953, 1990.

[3] H. J. Rothe. Lattice Gauge Theories. World Scientific Publishing Co. Pte. Ltd., Singapore, 1992.

[4] G. P. Lepage and P. B. Mackenzie. Viability of Lattice Perturbation Theory. Physical Review D, 48:2250, 1993.

[5] C. T. H. Davies, K. Hornbostel, G. P. Lepage, A. J. Lidsey, C. J. Morningstar, J. Shigemitsu and J. Sloan. Precision Υ Spectroscopy from Non-relativistic Lattice QCD. Physical Review D, 50:6963, 1994.

[6] C. T. H. Davies, K. Hornbostel, G. P. Lepage, A. J. Lidsey, J. Shigemitsu and J. Sloan. Precision Charmonium Spectroscopy from Lattice QCD. Physical Review D, 52:6519, 1995.

[7] M. Alford, W. Dimm, G. P. Lepage, G. Hockney and P. B. Mackenzie. QCD on Coarse Lattices. Nuclear Physics B (Proceedings Supplement), 42:787, 1995.

[8] H. R. Fiebig and R. M. Woloshyn. Light Hadron Masses with a Tadpole-improved Next-nearest-neighbour Lattice Fermion Action. Report Number hep-lat/9603001.

[9] M. Alford, T. Klassen, G. P. Lepage. The D234 Action for Light Quarks. Lattice 1995:370, 1995.

[10] S. Collins, R. G. Edwards, U. M. Heller and J. Sloan. Quenched SU(3) Hadron Spectroscopy using Improved Fermionic and Gauge Actions. Lattice 1995:366, 1995.

[11] J. Sexton, A. Vaccarino, D. Weingarten. Numerical Evidence for the Observation of a Scalar Glueball. Physical Review Letters, 75:4563, 1995.

[12] C. J. Morningstar and M. Peardon. The Scalar Glueball from a Tadpole-improved Action. Nuclear Physics B (Proceedings Supplement), 47:258, 1996.

[13] A. Hasenfratz and P. Hasenfratz. The Scales of Euclidean and Hamiltonian Lattice QCD. Nuclear Physics B, 193:210, 1981.

[14] F. Karsch. Finite Size Effects in Euclidean Lattice Thermodynamics for Non-interacting Bose and Fermi Systems. Nuclear Physics B, 205:239, 1982.

[15] G. Burgers, F. Karsch, A. Nakamura, and I. O. Stamatescu. QCD on Anisotropic Lattices. Nuclear Physics B, 304:587, 1988.

[16] M. Alford, T. R. Klassen, G. P. Lepage, C. J. Morningstar, M. Peardon, N. H. Shakespeare and H. Trottier. QCD on Anisotropic Lattices. Unpublished, to be submitted for publication.

[17] C. J. Morningstar and M. Peardon. SU(3) Glueballs on Coarse, Anisotropic Lattices. Report Number hep-lat/9608050.

[18] M. Teper. An Improved Method for Lattice Glueball Calculations. Physics Letters B, 183:345, 1986.

[19] M. Albanese et al (APE collaboration). Glueball Masses and String Tension in Lattice QCD. Physics Letters B, 192:163, 1987.

[20] A. Hulsebos, A. C. Irving, A. McKerrell, C. Michael, P. S. Spencer and P. W. Stephanson. SU(2) Potentials From Large Lattices. Nuclear Physics B, 394:509, 1993.

[21] C. N. Yang and R. Mills. Conservation of Isotopic Spin and Isotopic Gauge Invariance. Physical Review, 96:191, 1954.

[22] M. E. Peskin and D. V. Schroeder. Introduction to Quantum Field Theory. Addison-Wesley Publishing Company, Inc., Reading Massachusetts, 1995.

[23] C. Michael and S. J. Perantonis. Potentials and Glueballs at Large Beta in SU(2) Pure Gauge Theory. Journal of Physics G, 18:1725, 1992.

[24] S. Gasiorowicz and J. L. Rosner. Hadron Spectra and Quarks. American Journal of Physics, 49:954, 1981.

[25] B. Efron. Computers and the Theory of Statistics: Thinking the Unthinkable. Society for Industrial and Applied Mathematics Review, 21:460, 1979.

[26] G. S. Bali, C. Schlichter and K. Schilling. Observing Long Color Flux Tubes in SU(2) Lattice Gauge Theory. Physical Review D, 51:5165, 1995.

[27] K. Symanzik. Continuum Limit and Improved Action in Lattice Theories. Nuclear Physics B, 226:187, 1983.

[28] M. Lüscher and P. Weisz. On-shell Improved Lattice Gauge Theories. Communications in Mathematical Physics, 97:59, 1985.

[29] S. Elitzur. Impossibility of Spontaneously Breaking Local Symmetries. Physical Review D, 12:3978, 1975.

[30] G. P. Lepage. Private Communication.

[31] W. B. Rolnick. The Fundamental Particles and Their Interactions. Addison-Wesley Publishing Company, Inc., Reading Massachusetts, 1994.

[32] C. Michael and M. Teper. Towards the Continuum Limit of SU(2) Lattice Gauge Theory. Physics Letters B, 199:95, 1987.

[33] S. Perantonis, A. Huntley and C. Michael. Static Potentials from Pure SU(2) Lattice Gauge Theory. Nuclear Physics B, 326:544, 1989.

[34] U. Wolff. Comparison Between Cluster Monte Carlo Algorithms in the Ising Model. Physics Letters B, 228:379, 1989.

[35] T. Moretto and M. J. Teper. Glueball Spectra of SU(2) Gauge Theories in Three-Dimensions and Four-Dimensions: A Comparison with Isgur-Paton Flux Tube Model. Report Number hep-lat/9312035.